

The Bisha Volcanic-Associated Massive Sulfide Deposit, Western Nakfa Terrane, Eritrea

C. TUCKER BARRIE,[†]

29 Euclid Avenue, Ottawa, Ontario, Canada K1S 2W2

F. WILLIAM NIELSEN,

Newsun Resources Ltd., 901-141 Adelaide St. West, Toronto, Ontario, Canada M5H 3L5

AND CLAUDE H. AUSSANT

Taiga Consultants Ltd., #4, 1922 9th Avenue SE, Calgary, Alberta, Canada T2G 0V2

Abstract

The Neoproterozoic Bisha volcanic-associated massive sulfide deposit (VMS) is a large (>39 million metric tons (Mt)) relatively high grade Zn-Cu-Au-Ag deposit in a newly discovered VMS district in western Eritrea. The host stratigraphic section comprises a large, possibly coeval and cogenetic intrusion known as the Bisha Gabbroic Complex, ~3 km downsection, a series of mafic to felsic tuffs with minor flows and minor sedimentary rocks in the proximal footwall, and felsic flows, fine tuffs, and volcanic-derived siliciclastic rocks in the proximal hanging wall. Minor siliceous exhalite units extend for several kilometers along strike and are present upsection. Two other VMS deposits are present along strike: Bisha Northwest, 1.5 km to the north-northwest, and Harena, 9.5 km to the south-southwest; additionally, a large, lower grade VMS deposit, Hambok, is present ~15 km to the southwest.

The Bisha deposit is a single, nearly inclusion and dike-free lens, 1.2 km along strike, that has been folded and affected by significant, near-surface oxidation and supergene processes. The deposit and host strata form an overturned synform within a probable, west-over east, kilometer-scale nappe structure. It would appear that the strata have been folded and thrust against the gabbroic complex which behaved as a competent buttress during deformation.

The oxidation and supergene enrichment have led to the development of four mineralogically and spatially distinct ore types or zones. The hematite-goethite-quartz gossan, from 0- to ~30-m depth, has high gold, silver, and lead contents, with native gold, argentiferous gold, electrum, anglesite, and lesser cerrusite. The kaolinite-quartz-sulfate zone occurs at ~25- to 35-m depth, and also is enriched in gold, silver, and lead, and has the same ore mineralogy as the gossan; additionally it has minor chalcocite and minor to trace amounts of unusual Zn-Pb-Fe carbonate and sulfate minerals. The supergene sulfide zone is present from ~35- to 65-m depth and has significant copper enrichment, with predominant chalcocite, and lesser digenite, covellite, and bornite, along with pyrite, minor pyrrhotite, anglesite, and gangue minerals. The primary massive sulfide, from ~65- to more than 450-m depth, has a significant volume of zinc-rich ore and a typical VMS sulfide assemblage of pyrite, sphalerite, chalcopyrite, and minor to trace galena, pyrrhotite, tetrahedrite, tennantite, arsenopyrite, barite, and gangue.

The average ore and trace metal contents of the four ore types are calculated from an extensive assay and whole-rock geochemical database. The average metal contents for primary massive sulfide are comparable to that of other bimodal-siliciclastic deposits using an extended, primitive mantle-normalized plot. The ore metals, Cu, Pb, Zn, Au, and Ag, are 2.5 to 3 orders of magnitude higher than average continental crust, whereas the trace metals are more variable. Manganese is significantly depleted in comparison to the average crustal value.

Moderate to strong chloritic alteration and stringer sulfide veins are present in footwall felsic and intermediate tuffs along the entire strike length, immediately east of the eastern massive sulfide lens. This is highlighted using a chlorite alteration index, in wt percent: $(\text{MgO} + \text{FeO})^* 100 / (\text{MgO} + \text{FeO} + \text{CaO} + \text{K}_2\text{O} + \text{Na}_2\text{O})$. In addition, the chloritic footwall is depleted in silica, alkali, and alkaline earth elements, and europium. In contrast, these elements are enriched in the hanging-wall tuffs, indicating that the Bisha hydrothermal system continued after deposition of the tuffs.

Primary geochemistry of mafic to felsic volcanic and nearby intrusive rocks, including the Bisha Gabbroic Complex, indicate a bimodal igneous suite, with evidence for cogenetic and possibly coeval volcanic and intrusive rocks. The suite has tholeiitic to transitional calc-alkalic affinities, with mantle plume-influenced, primitive arc signatures for least altered basalts. Lead isotope ratios of galena and anglesite mineral separates from the Bisha, Bisha Northwest, and Harena deposits have model ages that range from 790 to 770 Ma. This is in contrast to a lead model age of ~720 Ma for the Adi Nefas VMS deposit in the eastern Nakfa terrane and to galena from a nearby gold vein deposit at ~490 Ma. The model ages for the Bisha area VMS deposits indicate that these deposits and their host rocks formed early during the development of the 850 to 550 Ma Nakfa terrane.

[†] Corresponding author: e-mail, barriect@sympatico.ca

Introduction

THE BISHA volcanic-associated massive sulfide (VMS) deposit was discovered in 1998 by systematic prospecting, geologic mapping, and stream sediment sampling in western Eritrea. Sampling of the surface gossan in 1999 yielded several high-grade samples, including one with 30.4 ppm Au, 18 ppm Ag, 0.20 percent Cu, and 1.01 percent Pb, which provided the impetus for an initial drill campaign. Drilling confirmed the discovery in November 2002, with the most significant intercept of 11.3 m at 16.5 ppm Au, 475 ppm Ag, 3.6 percent Cu, and 8.3 percent Pb, in iron oxide-sulfate-clay gossan near the surface. The initial drill program was followed by systematic geologic, geochemical, and geophysical exploration over a large prospecting license, which located two other significant deposits: Bisha Northwest in 2003, 1.5 km to the north-northwest, and Harena in 2005, 9.5 km to the south-southeast. Concurrent exploration in adjacent areas led to the discovery of the Hambok deposit, 13 km to the southwest (Sanu Resources press release, March, 2006), and other significant gossans. Thus, a new VMS district, herein termed the Bisha VMS district, has emerged in the Neoproterozoic volcanosedimentary terrane of western Eritrea.

Presently, the Bisha deposit has 39.01 million metric tons (Mt) of base and precious metal resources in all categories (Table 1). Much of the value of the deposit is within 65 m of the surface, in a gold-enriched gossan cap ("oxides") and a relatively shallow, chalcocite-bearing supergene blanket ("supergene Cu") immediately under the gossan. These zones overlie primary massive sulfide lenses that extend to at least 450-m depth. In addition to copper, zinc, gold, and silver, the deposit contains significant lead, and cadmium.

This contribution presents the geology and geochemistry of the Bisha VMS deposit and host rocks and places this deposit and nearby discoveries into a geotectonic context within the Nubian shield in northeast Africa. The Neoproterozoic geology is emphasized here, as the geologic events related to

primary mineralization occurred during this time. Cretaceous and Tertiary events related to the opening of the Red Sea are important regionally, but these are manifested only as minor faults and dikes in this area. Tertiary to recent weathering is very important, and this is discussed in the context of supergene sulfide and gossan formation.

It is noteworthy that the Bisha discovery will have a particularly high impact on the local populace and the country. The in situ metal value of the Bisha deposit is more than twice the gross domestic product of Eritrea ($\$US4.47 \times 10^9$, 2005 estimate: CIA World Factbook, 2006, www.cia.gov/library/publications/the-world-factbook/), one of the poorest countries in the world. The development of this deposit will lead the development of a new and modern mining industry in Eritrea.

Regional Geology:

VMS Deposits of the Arabian-Nubian Shield

The ~0.85 to 0.55 Ga Arabian-Nubian shield is a moderate-sized Precambrian (Cambrian) shield ($\sim 1.4 \times 10^6$ km²) composed of granitoid-greenstone belt terranes and mid-crustal gneissic terranes that underlie parts of Egypt, Sudan, Eritrea, Ethiopia, Israel, Jordan, Saudi Arabia, and Yemen, on either side of the Red Sea (Fig. 1). It represents the northern sector of the East African orogen, with supracrustal and mid-crustal rocks of similar age extending intermittently to the south into Mozambique and to southern Madagascar (Stern, 1994). In Eritrea, the Neoproterozoic basement has been divided into four terranes on the basis of distinct stratigraphic and structural characteristics, including: the Barka terrane to the far west (predominantly amphibolite-grade metasedimentary and mafic gneisses), the Hagar terrane to the north (principally mafic metavolcanic rocks, including ophiolite-like assemblages), the Nakfa terrane, the largest of the four (granitoid-greenstone belts and syn- to post-tectonic granitoid rocks), and the Arig terrane to the east (granitoid and metasedimentary

TABLE 1. Measured and Indicated, and Inferred Resources of the Bisha deposit¹

	Cut-off	Million tons	Au (g/t)	Ag (g/t)	Cu (%)	Zn (%)
Measured and indicated						
Oxides ²	0.5 g/t Au	4.800	7.02	30.2	0.09	0.08
Supergene Cu	0.5% Cu	7.503	0.72	32.3	3.96	0.12
Primary	2.0% Zn	8.576	0.76	59.5	1.06	9.19
Primary	2.0% Zn	1.663	0.75	31.4	0.79	3.09
Primary Zn	<2.0% Zn	4.744	0.67	33.2	1.15	1.01
		>0.5% Cu				
Total		27.286				
Inferred						
Oxides ²	0.5 g/t Au	0.600	2.85	17.5	0.03	0.02
Supergene Cu	0.5% Cu	0.206	0.48	21.1	1.94	0.03
Primary	2.0% Zn	6.803	0.65	53.3	0.83	8.42
Primary Zn	2.0% Zn	0.510	0.62	36.5	1.02	3.29
Primary	<2.0% Zn	4.147	0.68	37.3	0.99	0.87
		>0.5% Cu				
Total tons		11.726				

¹ From AMEC Canada prefeasibility report for Nevsun Resources (2006)

² Includes hematite-goethite-quartz gossan and kaolinite-quartz-sulfate zone

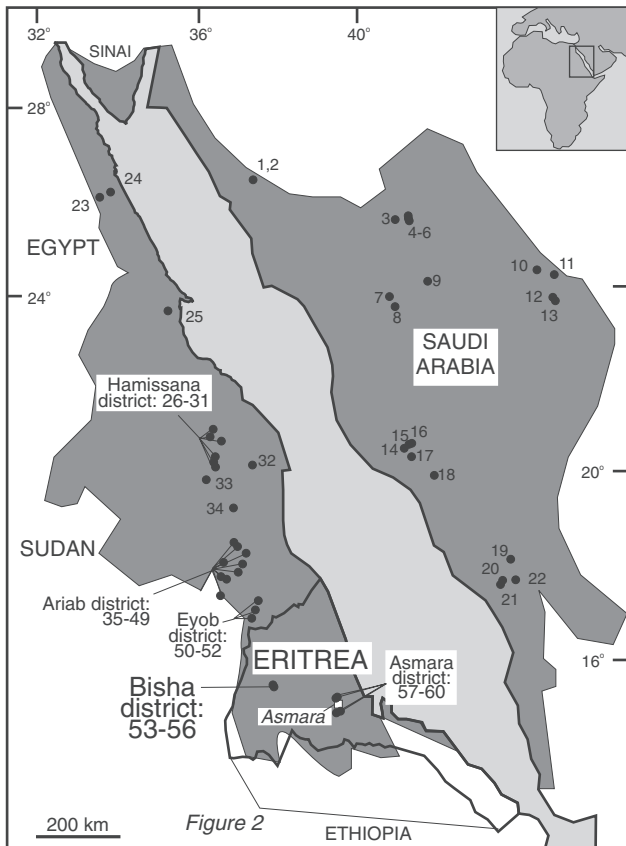


FIG. 1. Location of the Bisha VMS district and other VMS deposits in the Arabian-Nubian shield, Saudi Arabia: 1 = Ash Shizm, 2 = Jabal Ash Shizm, 3 = Nuqrah, 4 = Nuqrah North, 5 = An Nimahr, 6 = Nuqrah South, 7 = Jabal Sayid, 8 = Umm Ad Damar, 9 = As Safra, 10 = Ar Ridaniyah, 11 = Khnaiguiyah, 12 = Al Amar, 13 = Umm Ash Shalahib, 14 = Shaab At Tare, 15 = Wadi Bidah, 16 = Gehab, 17 = Rabathan, 18 = Jadma, 19 = Al Masane, 20 = Farah Garan, 21 = Kutam, 22 = Al Halahila. Egypt: 23 = Hamama, 24 = Abu Marawat, 25 = Um Samuiki. Sudan: 26 = Uar, 27 = Hamissana, 28 = Onib, 29 = Tbon, 30 = Eigiet, 31 = Adarmo, 32 = Gebiet, 33 = Bir Katieb, 34 = Serakoit, 35 = Tobay, 36 = Tibiry, 37 = Kalkoi, 38 = Igarairi, 39 = Shulai, 40 = Mandilu, 41 = Ashash, 42 = Hadal Auatib, 43 = Talaidrut, 44 = Ganeat, 45 = Oderuk, 46 = Kamoeb, 47 = Hassai, 48 = Adaimet, 49 = Tongi, 50 = Tohamyam, 51 = Abu Samar, 52 = Eyob. Eritrea: 53 = Bisha, 54 = Bisha Northwest, 55 = Harena, 56 = Hambok, 57 = Adi Nefas, 58 = Emba Derho, 59 = Debarwa, 60 = Adi Rassi (see Barrie and Hannington, 1999, and Franklin et al., 2005).

rocks; Fig. 2; Berhe, 1990; Teklay, 1997; Drury and de Sousa Filho, 1998). Mapping of the Hagar and Barka and terranes, in northwestern Eritrea indicated consistent west-over east thrust faults, particularly near the terrane boundaries (Drury and De Souza Filho, 1998). Almost all of the volcanic-sedimentary rocks of the Nakfa terrane strike north-south (± 25 degrees), and there is a significant volume of syn- to post-tectonic granite between the western and eastern halves. The Bisha VMS district (Bisha, Bisha Northwest, Harena, Hambok) and the Asmara VMS district (Adi Nefas, Debarwa, Emba Derho, Adi Rossi) are within the western and eastern parts of the Nakfa terrane, respectively.

There are at least 60 VMS deposits present in the Arabian-Nubian shield (Fig. 1). Although there are several types, the majority of the VMS deposits have host rocks with a significant felsic component and with barite present (e.g., bimodal-felsic

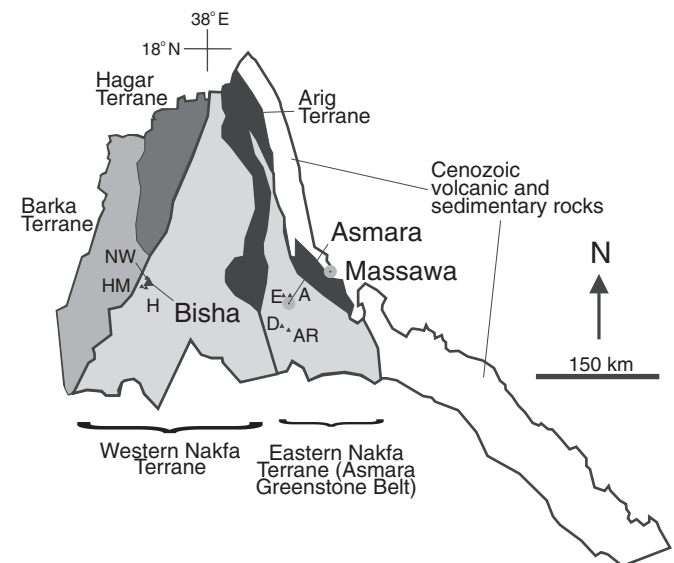


FIG. 2. Neoproterozoic terranes of Eritrea (from Teklay, 1997) with VMS deposits: Bisha = as labeled, NW = Bisha Northwest, H = Harena, HM = Hambok, E = Emba Derho, A = Adi Nefas, D = Debarwa, and AR = Adi Rossi.

or Kuroko-type: Sato, 1974; Barrie and Hannington, 1999; Franklin et al., 2005), consistent with evolved volcanic- and back-arc settings. Because of the arid environment, many have been subjected to near-surface oxidation and supergene enrichment so that gold and copper are relatively enriched at shallow depths, making them favorable targets for exploration from an economic standpoint.

Local Geology

The western Nakfa terrane near Bisha comprises basin- and range-style topography, with intrusive rocks commonly coring the north-trending ranges, and flat valley floors underlain by volcanic and sedimentary rocks. The area is arid and has been subjected to significant weathering and oxidation. Exposures in the valley floor are uncommon, and generally limited to the bases of the adjacent hills.

Bisha Gabbroic Complex

The geology of the Bisha region (Fig. 3) is dominated by the Bisha Gabbroic Complex, a 275-km², partly layered intrusion that forms high hills in the southern and central parts of the property. The complex extends in a north-northeast-south-southwest orientation for 35 km and has a maximum east-west width of ~12 km (south of the property). Medium- to coarse-grained cumulate gabbroic rocks predominate, with lesser gabbro-norite, pyroxenite, and ferroan gabbro containing up to 8 vol percent Fe-Ti oxides. Decimeter-scale cumulate layering is apparent locally and is likely common in the intrusion. Much of the gabbro is relatively fresh, with only minor hairline fractures filled with a quartz-clay-epidote \pm carbonate mineral assemblage. Near the gabbro margins, sporadic outcrops have more prominent alteration, including fracture-controlled and pervasive moderate epidote alteration. Felsite is present adjacent to the gabbroic intrusion in several locations. The felsite is up to 3 km thick along the

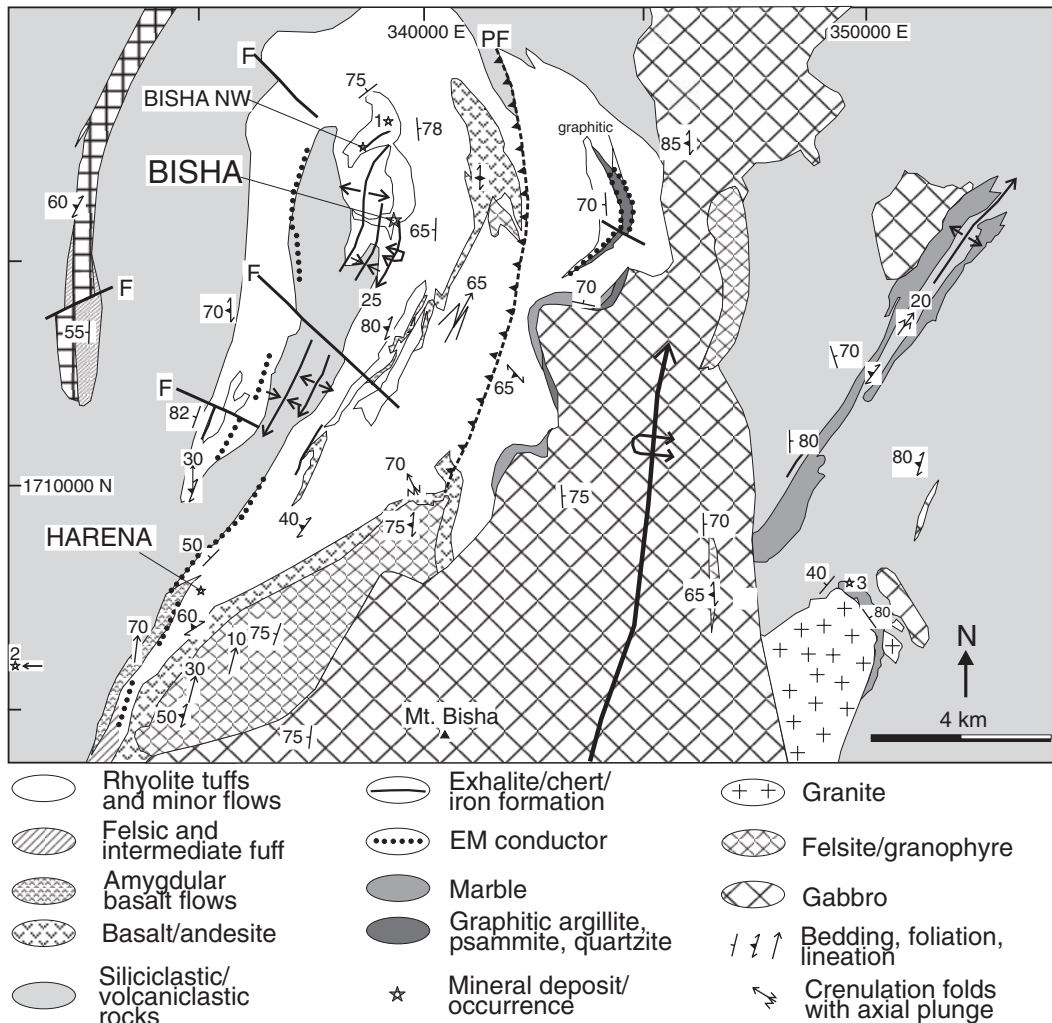


FIG. 3. Geology of the Bisha area ($15^{\circ} 24' N$, $37^{\circ} 30' E$). In addition to the Bisha, Bisha Northwest, and Harena VMS deposits, there are (labeled): Bisha North stringer occurrence (1); Hambok VMS deposit, 2 km west of map area (2), and the Okreb copper-gold skarn and vein deposits (3). The Bisha Gabbroic Complex is the main gabbroic mass that includes Mount Bisha.

western side of the Bisha Gabbroic Complex. It is generally fine grained but locally has granophyric textures. Along the northeastern side, the felsite has agmatitic and local mixed magma textures with mafic and gabbroic material, suggesting that it is coeval or nearly coeval with parts of the gabbroic complex. The Bisha Gabbroic Complex is largely concordant with strata along its western contact. Contacts with metasedimentary rocks along the eastern side are not present, and it is unclear whether there is a fault contact or the contact is intrusive and discordant. Sporadic gabbro outcrops are present in low-lying areas north of the property map area for several kilometers, and airborne geophysical trends indicate that the gabbro continues in this direction.

Volcanic-sedimentary stratigraphy

Overlying the Bisha Gabbroic Complex, the stratigraphic section comprises, from base to top: (1) shallow-water carbonates (calcareous and dolomitic, and with calc-silicate minerals locally near the Bisha Gabbroic Complex), quartzites

(locally crossbedded) and psammities, with units tens of m thick; (2) intermediate and felsic lapilli and ash crystal lapilli tuffs, with units up to hundreds of m thick; (3) mafic tuffs, minor locally amygdaloidal mafic flows and hyaloclastite with units up to tens of m thick; and (4) fine-grained siliciclastic rocks, with units tens to hundreds of m thick (Figs. 4–6). Volcanic rocks comprise ~75 percent of the stratigraphic section between the deposit and the gabbroic complex and ~25 percent in the strata upsection from the deposit for several kilometers to the southwest and west. Felsic dikes are also present but uncommon at surface. They appear as rhyolite porphyry or as granitic rocks; in one location, stellate clusters of a green amphibole are observed.

In the southeastern part of the property near the historical Okreb mine, the strata are cut by a granitic intrusion and gold-copper-bearing quartz veins, and skarn is present in carbonate-bearing strata.

Most of the felsic volcanic rocks contain lapilli fragments less than 5 cm in diameter. There are a few coarse lapilli and

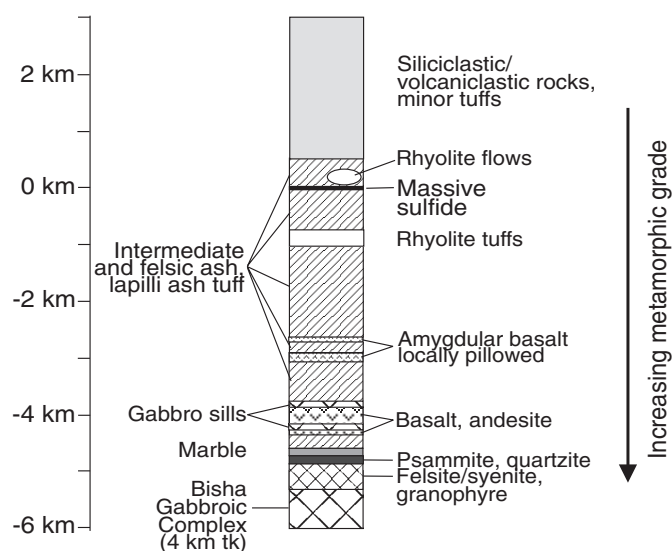


FIG. 4. Regional stratigraphic section, assuming that marble and quartzite units adjacent to the Bisha Gabbroic Complex are the stratigraphic base and that the stratigraphic section broadly faces to the northwest. Gabbro and/or basalt porphyry and felsic sills up to 200 m thick are present within 2.5 km of the main Bisha Gabbroic Complex contact. The section is cut by thinner felsic and mafic dikes (not shown).

agglomerate fragmental units up to 10 m thick, ~2 km down-section and southeast of the Bisha deposit. Rhyolitic tuffs are common, with lesser dacite tuff, and minor rhyolite blocky flows and agglomerates are present immediately west of the Bisha and Bisha Northwest deposits. Approximately half of the rhyolite outcrops contain discernible volcanic features, whereas the remainder are quartz-sericite-chlorite (\pm clay) phyllites and schists. Basalt and minor andesite are present principally down-section from the Bisha horizon, but in the Harena area, basalt also occurs in the hanging wall to the west. Away from hydrothermal alteration, massive and locally pillowed flows and flow breccias are discernible, whereas near the Bisha deposit, chloritic mafic tuffs, phyllites, and schists predominate. The hanging-wall strata are less well constrained due to poor exposure in the valley floor to the west or to significant oxidation near the deposit that masks primary textures. The hanging-wall strata are predominantly fine-grained tuffs and volcaniclastic rocks of intermediate to felsic composition, extending west from the deposit area for several kilometers and to the southwest. The volcanic and sedimentary strata are at prehnite-pumpellyite to mid-greenschist facies metamorphic grade, which generally increases toward the Bisha Gabbroic Complex.

In the lower part of the section, the carbonates and quartzites with locally preserved crossbeds are interpreted to indicate shallow, near-shore depositional environments. These are overlain by volcanic tuffs and flows, the main ore horizon, including minor siliceous exhalites, and eventually by fine tuffs gradational with volcanic-derived, locally turbiditic siliciclastic rocks. The stratigraphic sequence is consistent with a progressively deepening seawater environment.

Structural geology

The strata across the Bisha property are commonly foliated, with phyllic, schistose, and locally gneissic penetrative fabrics.

Gneissosity increases toward the Bisha Gabbroic Complex, and L-S fabrics are apparent in ~20 percent of the outcrops within 3 km of the complex. Reliable facing directions are uncommon due to weathering and oxidation, particularly in hydrothermally altered outcrops near the deposit. They are more common in the margins of the gabbroic complex and in intercalated metasedimentary layers. From the facing directions and bedding-cleavage relationships, the strata in the western half of the area generally face west, with north-trending, upright, and locally overturned folds on a scale of tens to hundreds of meters. Detailed surface mapping of gossans in the vicinity of the Bisha deposit indicate the presence of isoclinal fold hinges that open broadly to the south, with fold axes that plunge shallowly to the north.

Three foliation fabrics have been detected at surface (C. Greig, consultant, pers. commun., 2005; and W.F. Nielson and C. Aussant, unpub. report for Nevsun Resources, 2005, 350 p.). The earliest S_1 fabric is well developed at surface in the vicinity of the Bisha and Bisha Northwest deposits and is generally parallel or subparallel to bedding where bedding can be discerned. It is a flattening fabric that is manifested as schistosity, particularly in altered tuffs. The second and third fabrics are generally difficult to discern but are found locally in decimeter-scale, parasitic isoclinal fold hinges, and provide evidence for refolded folds, at least locally.

A kilometer-scale nappe with a west-over-east displacement is interpreted from the folds and from prominent airborne magnetic and electromagnetic trends, and this is supported by lithologic trends (Fig. 3). Within this nappe, the strata and folds are locally overturned, including at the Bisha deposit (see below). To the east and southeast from Bisha, the Bisha Gabbroic Complex forms the core of a north-plunging anticline. From the initial mapping in the area, it would appear that the more competent Bisha Gabbroic Complex acted as a buttress to the Bisha deposit stratigraphy and nappe during west-over-east thrusting and amalgamation of the Neoproterozoic tectonostratigraphic terranes in this region.

The Bisha Deposit

Geology

The host rocks of the Bisha deposit are principally felsic and intermediate lapilli, ash, and crystal (fine- to medium-grained feldspar, quartz, biotite, locally hornblende) ash tuffs (Fig. 6a, c) that are variably altered. Minor feldspar and quartz-feldspar felsic flows and flow breccias are present only to the west of the deposit. Generally the volcanic host rocks are difficult to correlate over distances of greater than 50 m in drill core, due to their variability in texture and thickness and the overprinting hydrothermal alteration. It is not possible to correlate footwall tuff beds to surface exposures due to the accentuation of penetrative fabrics in these hydrothermally altered and oxidized rocks at surface. Within the drill core, several units have distinctive mafic and felsic juvenile fragments, and these units correlate for up to 250 m. Felsic dikes, up to 5 m thick, are present in drill core but comprise <5 percent of the footwall and hanging-wall rocks. These dikes have up to 25 percent feldspar, quartz, and biotite phenocrysts and are generally fine grained. In the structural hanging wall to the west, massive

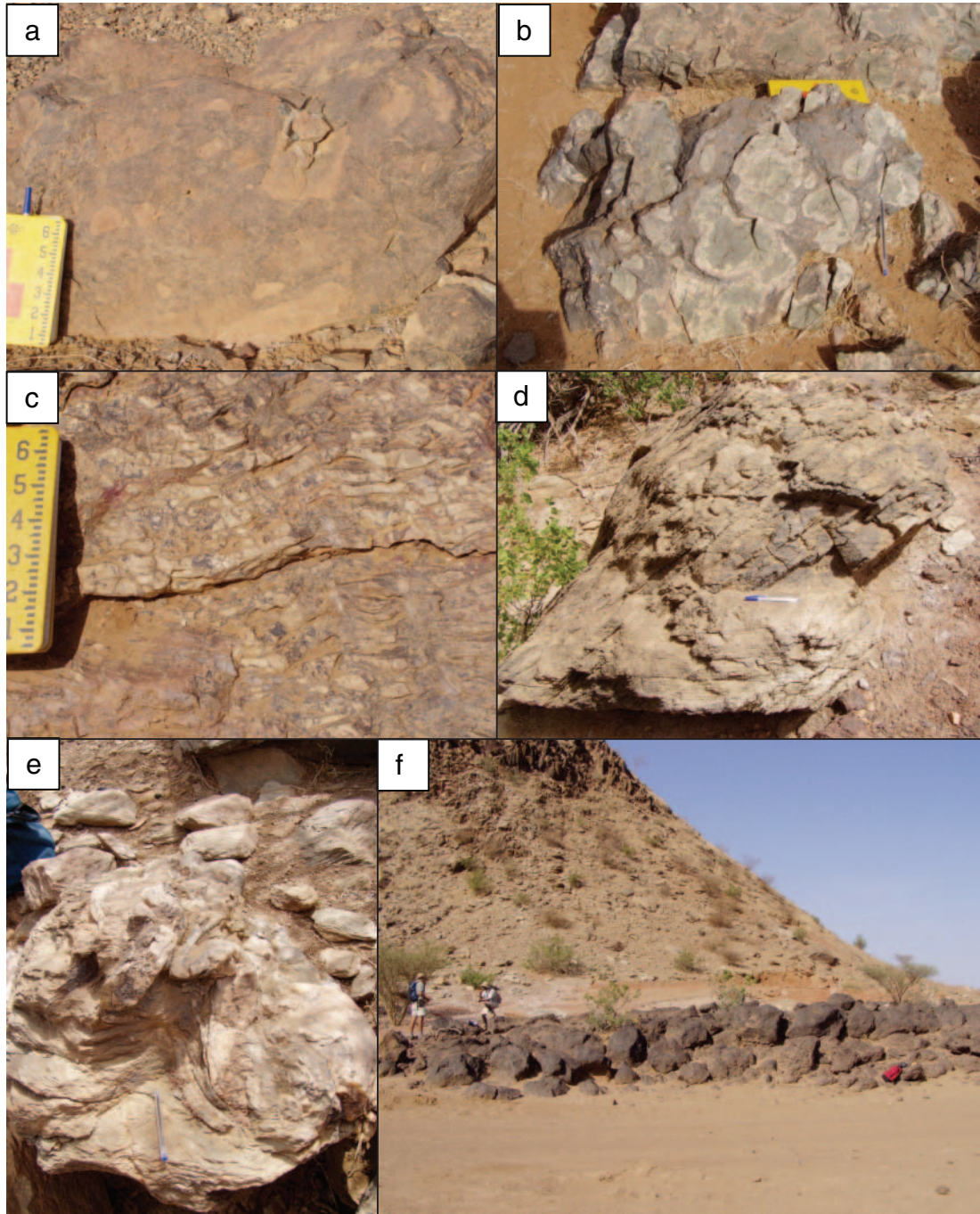


FIG. 5. Outcrop photographs in the Bisha area. a. Felsic fragmental, 2 km east and downsection from deposit. Notebook has scale in inches. b. Pillow basalt and coarse hyaloclastite basalt with bleached rims, 7 km south-southwest from deposit and ~350 m downsection from ore horizon. c. Flow banding in silicified rhyolite 250 m west of Bisha Northwest. d. Bedding (parallel to pen) and cleavage relationship in felsic tuffs, 150 m west of Bisha deposit. e. Ptygmatic folds in centimeter-scale exhalite layers within felsic tuff, immediately west of Bisha deposit. f. Prominent hematite-goethite gossan, the surface expression of the western lens in the northern half of the Bisha deposit.

felsic flows and flow breccias are present at thicknesses of up to 60 m (Fig 6b).

The Bisha VMS deposit is effectively a single sheet of massive sulfide up to 70 m in thickness that has been folded and partly overturned along a north-trending, steeply west dipping axis (Fig. 7). The eastern lens is on the eastern limb of

the fold, and the western lenses (north and south) are on the opposing western fold limb. The east and west lenses are separated from each other due to erosion and surficial oxidation processes; however, massive sulfide is continuous over the fold nose locally (Fig. 7), and oxidized material links them for several hundred m in the central part of the deposit. Sulfide

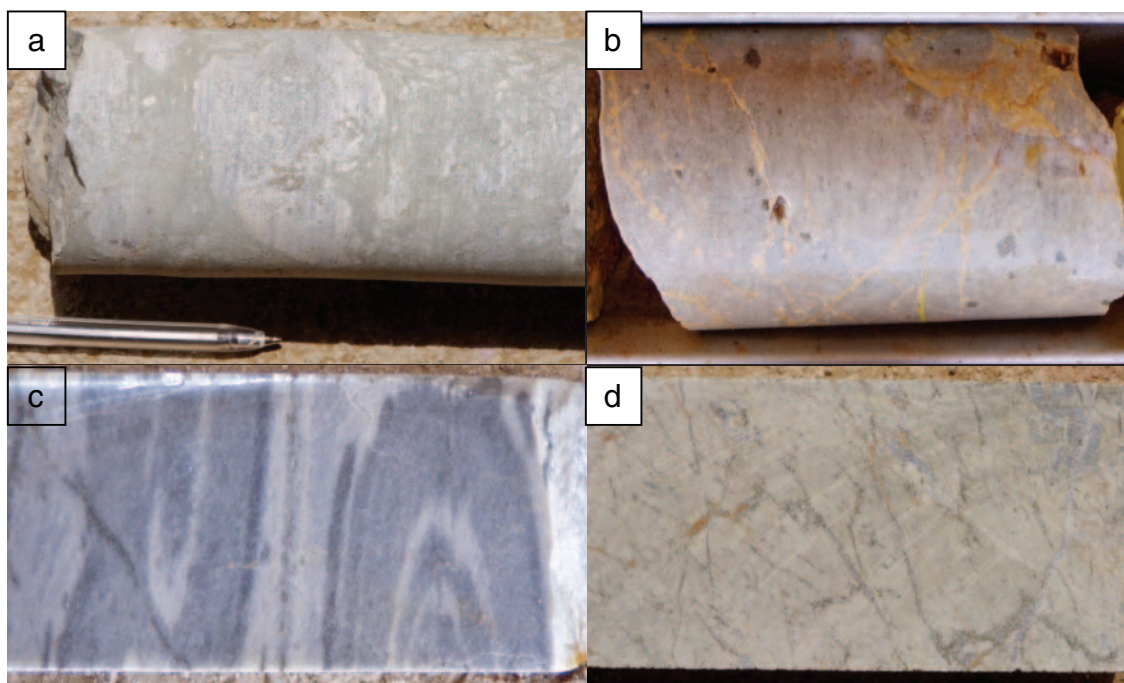


FIG. 6. Drill core photographs of the host rocks of the Bisha deposit. The drill core is 12 cm in diameter. a. Dacite fragmental tuff with moderate chlorite alteration in the ash- and crystal-rich matrix. Chloritic dacite tuffs are the principal host rock for the Bisha deposit. b. Massive, feldspar-phyric rhyolite with sparsely disseminated coarse pyrite, immediately west of the west lens. c. Sheath folds in dacite ash tuff between the west and east lenses. d. Pyrite stringers cutting sericitized dacite ash tuff in footwall to the west lens.

stringer veins (Fig. 6d) are ubiquitous in chloritic felsic and intermediate tuffs along the stratigraphic footwall to the eastern lens but are sporadically dispersed adjacent to the western lenses. The surface expression of the northern half of the Bisha deposit is manifested as prominent hematite-goethite-quartz gossans up to 25 m wide and extending for tens to hundreds of m. In places, the gossans stand in high relief up to 1.5 m above the adjacent alluvial floor (Fig. 5f). The southern half of the deposit lies beneath 3 to 20 m of alluvium.

The eastern lens is a nearly continuous sheet for over 1.2 km that faces west and dips 65° to 70° to the west. Evidence for a westerly facing direction is as follows: (1) primary (e.g., below the oxidized zone) massive sulfide is generally enriched in Zn to the west, reflecting the common enrichment of zinc at the tops of massive sulfide lenses (e.g., Sato, 1974); (2) strong chlorite alteration and sulfide stringer mineralization in felsic tuffs are ubiquitous and strong to the east and much less abundant west of the primary sulfide in the eastern lens at depth; (3) barium enrichment is much more common in tuffs west of the primary sulfide of the eastern lens at depth. The deepest drill holes in the southern half of the eastern lens have layered massive sulfide with high zinc contents and Zn/Cu ratios over two separate 5- to 10-m intervals, suggesting stacked massive sulfide lenses in this area.

The primary characteristics of the shallower western lenses are less clear due to near-surface oxidation and their unusual geometry. Zinc has been largely removed from the sulfide, and Cu, Pb, Au, and Ag are sporadically enriched by near-surface supergene and oxidation processes. A few deeper massive sulfide intersections in the western lenses, for example in

section 11715500N and in nearby sections, have Zn enriched near the base of the lens, suggesting that the western lens faces east, on the other side of an overturned synform from the eastern lens. Barium enrichment in tuffs consistently occurs at depth and east of the western lens but is generally absent to the west of the western lens. This is consistent with barite deposition above the massive sulfide lens after massive sulfide formation and prior to deformation.

These features (primary metal zonation, distribution of stringer sulfide and strong chloritic alteration, and orientation of barium enrichment relative to the massive sulfide lenses) are consistent with an overturned fold geometry, with the axial plane dipping steeply to the west, and with a north-trending axis that undulates but broadly plunges to the north through the Bisha Main area (Fig. 6).

Ore types, mineralogy, and metal distribution

There are four principal ore types that can be clearly divided into spatially distinct zones or volumes of rock. From the surface downward, they are (1) a hematite-goethite-quartz oxide zone, or gossan, from ~0- to 30-m depth (Fig. 8a); (2) a kaolinite-quartz-sulfate zone at ~25- to 35-m depth (Fig. 8b); (3) chalcocite-dominant supergene sulfide (~30-65 m; Fig. 8b); and (4) primary massive sulfide (~65 to more than 450 m; Fig. 8c, d). The gossan can be subdivided into brecciated and semimassive types; however, the mineralogy and metal contents of these two types are nearly identical. The primary sulfide is subdivided on the basis of Zn content (sphalerite abundance) and Cu content (chalcopyrite abundance) in Table 2. A fifth type of mineralization, not listed in

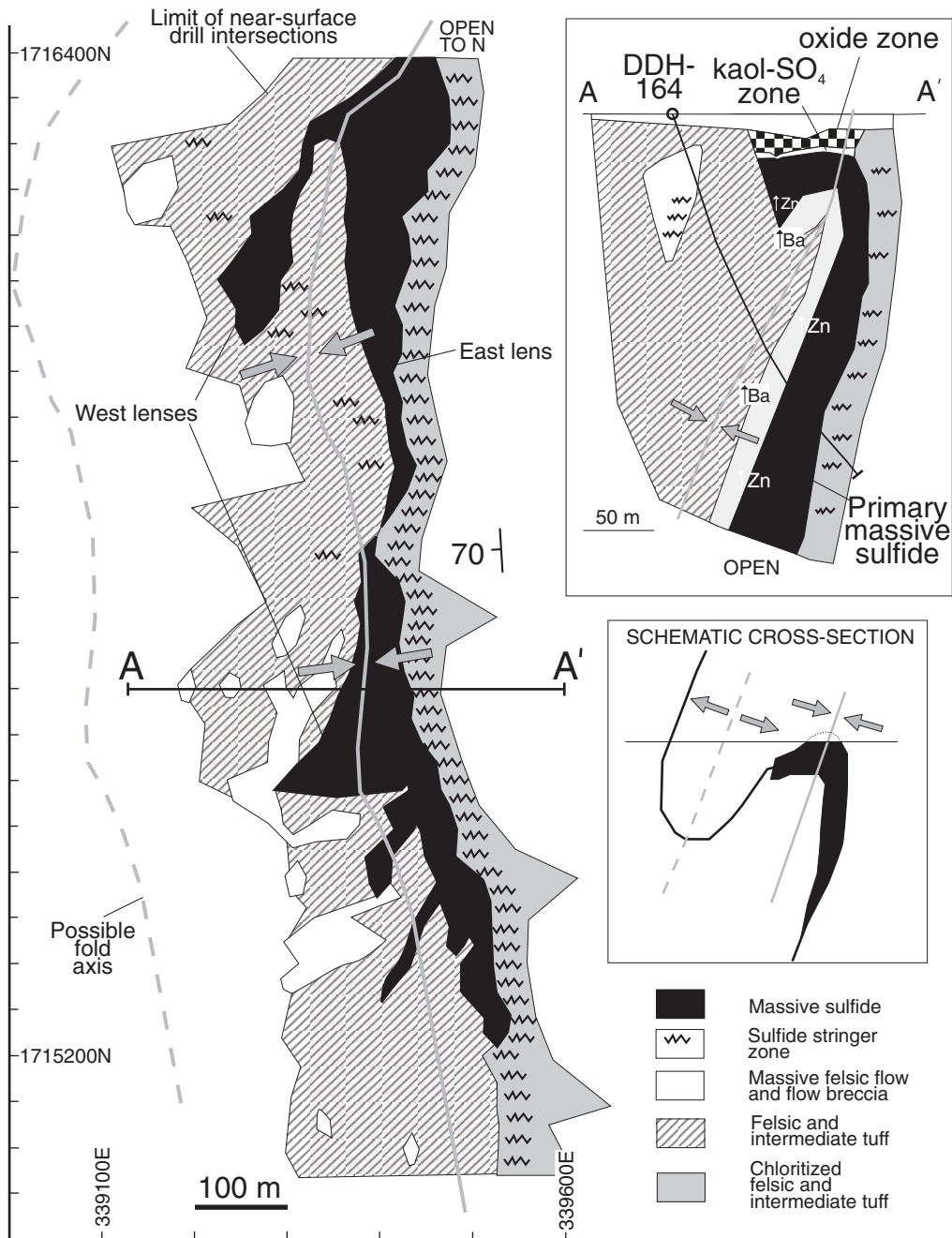


FIG. 7. Near-surface geology and cross section of the Bisha VMS deposit, based on 377 diamond drill holes. The north half of the deposit is under a gossan cap and up to 15 m of alluvium, whereas the southern half is under 15 to 30 m of alluvium. The plan map is from the highest intersections below gossan or alluvium. Cross section A-A' indicates where higher zinc is concentrated in massive sulfide intersections and where higher barium is present in altered tuffaceous host rocks. Stringer sulfide veins are present in nearly every drill hole that penetrates the stratigraphic footwall of the eastern lens but are uncommon on the western side of this lens. Drill hole DDH-164 projected from 50 m south onto section A-A'.

the resource calculation, is chalcocite-cemented alluvium and saprolite at the fringes of the deposit, particularly to the western, downslope side. This ore type represents a significant resource for copper, but it is not well defined in terms of resources (or in terms of geology) at this time.

The average metal contents for the main ore types are given in Table 2, with the hematite-goethite-quartz and kaolinite-quartz-sulfate types combined. Representative microprobe

data for the main ore minerals are given in Table 3. Representative ore and gangue textures are shown in Figures 8 and 9. A schematic mineralogical paragenetic sequence for these four ore types is presented in Figure 10a, and a schematic diagram of the metal contents for these zones is shown in Figure 10b.

Hematite-goethite-quartz oxide zone: The hematite-goethite-quartz oxide zone, or gossan, comprises a massive, dense

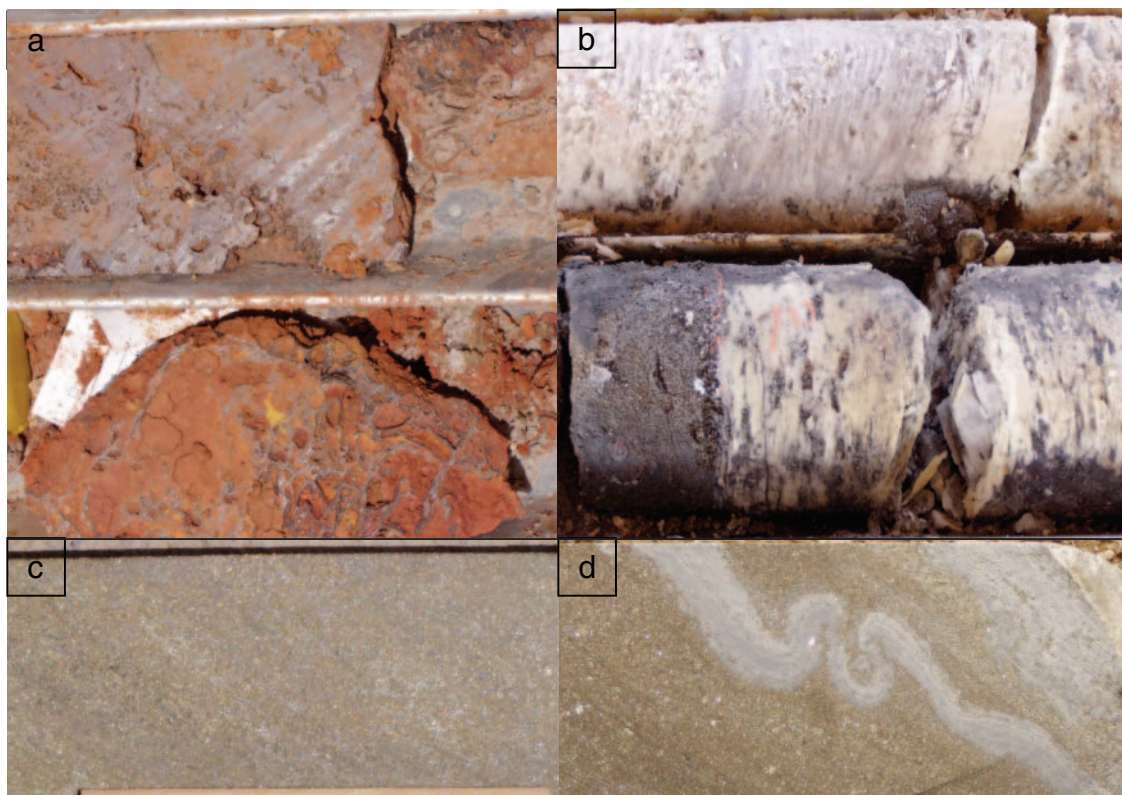


FIG. 8. Drill core photographs of massive sulfide and oxide ore types. The drill core is 12 cm in diameter. a. Hematite goethite gossan. Porosity is due to removal of carbonate and sulfate by acidic ground water. This interval has 5.4 ppm Au, 22 ppm Ag, 2.0 wt percent Pb, 1.2 wt percent Ba, and 0.9 wt percent As. b. Chalcocite-rich supergene massive sulfide intercalated with kaolinite-quartz after felsic ash tuff. c. Medium-grained, layered massive sulfide from the east lens. This interval contains 0.32 wt percent Cu, 28.3 wt percent Zn, 3.2 wt percent Pb, 1.2 ppm Au, and 106 ppm Ag. d. Ptygmatic folds in centimeter-scale exhalite at the stratigraphic top of the east lens, 30 m upsection from the previous photo.

hematite-goethite-dominant assemblage, with hematite more abundant near the surface. Gold and silver are the principal metals of value, and the main ore minerals are native gold, argentiferous gold, and pyargarite (Table 3, Figs. 9, 10). The gangue includes iron oxides, quartz, and other SiO_2 polymorphs including chalcedony and minor (2–5 vol %) opaline chalcedony; kaolinite, jarosite, gypsum, barite, and calcite; and accessory (1–2 vol %) to trace (<1 vol %) levels of alunite, cerrusite, anglesite, and native copper (Fig. 9). All primary sulfides have been destroyed, although void space after pyrite crystals is present locally. Multiple generations of botryoidal iron oxides and lesser carbonate and sulfate minerals fill void space (Fig. 9). Native gold is commonly found coating botryoidal or recrystallized hematite and goethite.

Kaolinite-quartz-sulfate zone: This zone has a characteristic leached appearance, with white to cream-colored, aphanitic to fine-grained kaolinite (\pm illite)-gypsum-alunite encasing fine- to medium-grained quartz grains. The rocks are commonly slippery or soapy to the touch due to aphanitic to fine-grained kaolinite (e.g., white material in Fig. 8b), interpreted to be highly altered and leached tuffaceous material. On average, samples from this zone contain more than 13 ppm Au and more than 170 ppm Ag (Table 2), and this material constitutes a very important component of the oxide zone resource. It also contains the highest proportion of lead of the four zones, which is principally in sulfate and carbonate

minerals. Ore minerals include chalcocite, chlorargyrite, and native gold (Figs. 9, 10); additional gangue minerals include siderite, calcite, gypsum, hematite, goethite, and minor to trace manganese oxide, arsenopyrite, and unusual carbonates and sulfates, including Zn-Pb-Mn siderite, cerrusite, barian anglesite, barian magnesite (norsethite?), and beudantite, a lead-arsenic hydrated sulfate, which generally occurs in oxidized zones above VMS deposits (Nieto et al., 2003). Malachite, azurite, and brochantite are notably absent in this zone (as well as absent from the gossan and supergene zones), despite the presence of carbonate and copper.

Supergene sulfide zone: Supergene sulfide ore is generally medium- to coarse-grained massive sulfide enriched in secondary copper minerals. It is more granular, with local cavities and vugs, and has a darker gray, dirtier appearance than primary massive sulfide. The darker coloring is due to a high proportion of dark gray, often sooty chalcocite. The granular, vuggy textures are due to the partial to complete dissolution of sphalerite, galena, and pyrite, and minor recrystallization or reprecipitation of iron sulfides (Fig. 9). Highly chalcocite-enriched supergene sulfide has a characteristic steel blue-gray color and values of up to 28.9 wt percent Cu over 9.7 m (DDH B-241 at 1716050N). Ore minerals include the aforementioned sulfides, as well as minor bornite, digenite, covellite, and minor to trace enargite, tetrahedrite, and tennantite; gangue includes iron sulfides (marcasite, secondary pyrite,

TABLE 2. Major and Trace Metal Contents of Different Types of Mineralization in the Bisha Deposit¹

Type	Hematite goethite oxide zone	Kaolinite sulfate zone	Supergene massive sulfide	Primary massive sulfide
<i>n</i>	732	216	2191	3768
Cu ² (wt %)	0.08	0.06	3.91	0.99
Zn ² (wt %)	0.07	0.02	0.12	5.72
Pb (wt %)	0.70	1.47	0.21	0.20
Au ² (ppm)	6.56	13.72	0.71	0.70
Ag ² (ppm)	28.8	171.8	32.0	47.5
Fe (wt %)	40.70	6.86	42.45	40.31
S (wt %)	0.62	2.39	45.39	44.16
Ba (wt %)	1.62	1.38	1.71	0.27
Ga ³ (ppm)	9.3	10.2	1.3	8.1
In ³ (ppm)	0.50	0.21	1.31	3.53
Cd (ppm)	5.2	5.0	18.2	176.5
As (ppm)	3680	689	1067	704
Sb (ppm)	152.6	41.9	24.7	28.3
Hg ⁴ (ppm)	(5.59)	(13.79)	(6.17)	(5.50)
Sn ³ (ppm)	44.2	4.6	9.1	6.1
Mo (ppm)	16.3	6.3	5.8	5.5
Mn (ppm)	76.6	41.6	42.5	370.8
Co (ppm)	7.6	7.2	105.8	113.8

¹ ICP analyses after 4 acid attack, Ba analyses may be low due to incomplete dissolution of barite; ALS-Chemex Laboratories, Vancouver, B.C.

² Values for oxide, supergene and primary taken from weighted average of measured, indicated, and inferred resource grades in Table 1

³ Average 9, 4, 9, and 12 representative samples for the four zones, respectively, using ICP-MS after 4 acid attack; ALS-Chemex Laboratories, Vancouver, B.C.

⁴ Calculated using 5 (ppm) for samples below 5 (ppm) detection limit

and pyrrhotite), quartz, chlorite, kaolinite; and minor to trace amounts of jarosite, barite, siderite, and calcite (Figs. 9, 10). Chalcocite is more abundant at higher levels, whereas digenite, covellite, and bornite are more common approaching the primary sulfides below.

Primary massive sulfide zone: Beneath the effects of oxidation and supergene enrichment, primary massive sulfide is present. Most of the primary massive sulfide is in the eastern lens, where fine- and medium-grained massive sulfide is locally layered with probable primary depositional layering. The primary massive sulfide contains most of the Zn resources in the deposit, as sphalerite has been partially or completely removed from the system in the overlying ore types (Table 2). The principal ore minerals comprise a typical VMS assemblage, with pyrite, sphalerite, chalcopyrite, minor galena and pyrrhotite, and accessory arsenopyrite, tetrahedrite, tennantite, and enargite (Figs. 9, 10). Tetrahedrite in the primary zone has high silver contents of 3.6 wt percent Ag ($n = 4$; Table 3). Gangue minerals include quartz, chlorite, sericite-muscovite, clay minerals, siderite, and ferroan carbonate, and minor to trace arsenopyrite, barite, and carbonate minerals. Magnetite is notably absent. Sphalerite-rich massive sulfide has up 22.0 wt percent Zn over tens of meters (e.g., 20.8-m interval in DDH B-155 at 1715625N; also with 1.04 wt % Cu, 0.79 wt % Pb, 0.88 ppm Au, 105.6 ppm Ag, and 0.07 wt % Cd).

Sphalerite is generally inclusion-free but some sphalerite exhibits very fine chalcopyrite blebs aligned along crystallographic axes (i.e., chalcopyrite disease). The sphalerite has low to moderate iron contents, averaging 3.96 wt percent Fe or 6.8 mol percent FeS ($n = 10$, Table 3). For comparison, sphalerite in primary massive sulfide in the giant Kidd Creek VMS deposit in Ontario has 12 mol percent FeS, whereas in the overlying turbidites and argillites, sphalerite has ~6 mol

TABLE 3. Average Electron Microprobe Analyses of

Mineral	Mineralization type	<i>n</i>	Fe	Cu	Zn	Cd	Ga	Ge	In	Se
Pyrite ²	Primary and Supergene	16	47.67	0.04	0.03	<0.01	0.01	<0.01	0.01	0.01
Pyrite (secondary)	Supergene	2	43.05	2.93	0.09	0.02	<0.01	<0.01	0.01	0.01
Pyrrhotite	Primary	2	60.89	0.16	0.12	<0.01	0.01	<0.01	<0.01	<0.01
Sphalerite	Primary	10	3.96	0.06	64.32	0.24	0.12	0.01	0.01	0.01
Galena	Primary	5	0.21	0.04	0.01	0.08	0.01	<0.01	0.01	0.10
Arsenopyrite	Primary and Supergene	11	36.02	0.09	0.02	0.01	<0.01	<0.01	0.01	0.24
Tennantite	Primary	6	5.84	41.72	2.99	0.03	<0.01	<0.01	<0.01	0.10
Tetrahedrite	Primary	4	4.53	35.86	2.72	<0.01	<0.01	<0.01	<0.01	0.03
Tetrahedrite (Ag)	Supergene	1	5.50	26.61	1.13	0.07	<0.01	<0.01	<0.01	<0.01
Chalcopyrite	Primary	6	30.76	34.20	0.08	<0.01	<0.01	0.01	0.01	0.01
Covellite	Supergene	3	0.81	66.00	0.01	0.02	0.03	<0.01	<0.01	0.01
Digenite	Supergene	7	0.29	76.46	0.04	0.01	0.01	0.01	0.01	0.02
Enargite	Supergene	6	1.32	47.45	0.03	0.02	<0.01	0.04	0.01	0.08
Gold	Oxide and kaol-sulfate	15	0.25	0.02	<0.01	<0.01	0.11	<0.01	<0.01	0.03
Gold-silver	Oxide and kaol-sulfate	3	0.40	0.02	<0.01	<0.01	0.11	<0.01	<0.01	0.03
Chlorargyrite	Oxide and kaol-sulfate	4	0.24	0.01	<0.01	0.15	<0.01	<0.01	<0.01	<0.01
Copper	Oxide and kaol-sulfate	3	0.21	97.15	<0.01	<0.01	<0.01	<0.01	<0.01	0.01
Beudantite ?	Oxide	2	24.43	0.14	<0.01	<0.01	<0.01	<0.01	<0.01	0.05
Hematite ³	Oxide	1	59.94	0.03	<0.01	<0.01	<0.01	<0.01	<0.01	0.05

¹ WDA using Cameca Camebax electron microprobe at Carleton University, Ottawa, Canada, by I. Kjarsgaard

² Sulfides and native elements analyzed at 25 kV and 30 nA with counting times of 10 to 20 s

³ Oxides analyzed at 25 kV and 26 to 30 nA with 10- to 20-s counting times

percent FeS (Hannington et al., 1999). Gallium, germanium, and indium concentrations were evaluated here, because of their potential to enhance the economics of the deposit. Sphalerite contains measurable gallium, averaging 0.12 wt percent Ga ($n = 10$; Table 3). Generally gallium contents in sphalerite are less than ~200 ppm. Along with indium (3+) and germanium (4+), gallium (3+) has coupled substitution with monovalent and divalent copper in the sphalerite crystal structure (Johan, 1988).

Metal distribution among the four ore types: Bisha presents a classic supergene oxidation profile for VMS deposits in weathered terrane. Assuming that originally, primary massive sulfide was present in the supergene, kaolinite-quartz-sulfate and oxide zones, the gains and losses in metals can be calculated from the data in Table 2. This is presented schematically in Figure 10b. Zinc, cadmium, and indium, elements that reside in sphalerite, are nearly completely stripped from the three upper zones. Copper is enriched threefold in the supergene zone but is nearly completely removed from the upper two zones. In complimentary fashion, gold and lead are significantly enriched in the upper two zones. In comparison to primary massive sulfide, gold is enriched 8.3× and 18.6× in the oxide and kaolinite-quartz-sulfate zones, respectively, and lead is enriched 2.6× and 6.5× for these two zones, respectively. Manganese is depleted 80 to 90 percent in the supergene and gossan zones in comparison to the primary massive sulfide.

Primary Igneous and Alteration Geochemistry

Whole-rock major and trace element geochemistry were used routinely during surface mapping and core logging to assist in rock identification and correlation, with over 600 surface and core samples analyzed by X-ray fluorescence and by inductively coupled plasma mass spectrometry (ICP-MS)

after lithium metaborate fusion. Details of the sampling procedures, analytical techniques, and standards for these data are described in Reddy and Brisebois (2004). Averages for least altered igneous rock types are given in Appendix 1. The least altered samples were screened on the basis of their hand specimen descriptions, petrography, their alkali, and loss on ignition contents (e.g., avoiding very low Na₂O, K₂O, and CaO contents and very high loss on ignition), and avoiding extreme values for other oxides and trace elements. Data for a suite of altered tuffs on either side of the eastern lens is given in Appendix 2. Data from the least altered rocks are shown in normalized plots in Figures 11 and 12, and a synthesis of the geochemical alteration near the massive sulfide using a chlorite alteration index is shown in Figure 13.

Geochemistry of less altered igneous rocks

Most of the less-altered rhyolite tuffs and flows have 70 to 78 wt percent SiO₂, 0.17 to 0.3 wt percent TiO₂, 160 to 220 ppm Zr, and La_N/Yb_N from 1.2 to 5.0 (Fig. 11a, App. 1). Less-altered dacites are clearly distinguished from basalts and rhyolites by their TiO₂ and Zr contents, which range from 0.38 to 0.6 wt percent and 120 to 200 ppm, respectively. They have 60 to 68 wt percent SiO₂ and La_N/Yb_N from 1.0 to 3.0 (Fig. 11b). A suite of feldspar and quartz feldspar porphyry dikes is chemically distinctive from the other felsic strata. These rocks have 68 to 74 wt percent SiO₂, 0.14 to 0.35 wt percent TiO₂, 3.2 to 4.2 wt percent Na₂O, 2.2 to 4.5 wt percent K₂O, and 175 to 208 ppm Zr and are characterized by steep REE patterns, and La_N/Yb_N 26 to 115 (Fig. 11b, App. 1). Two granite dike samples have similar geochemistry to the rhyolites, although one has appreciably lower Zr and TiO₂ contents, and higher U and Th contents, and may represent a highly fractionated equivalent of the rhyolites (Fig. 11b, App. 1). The

Sulfides and Other Minerals from the Bisha Deposit¹

Pb	Ag	Au	As	Sb	Te	Hg	Bi	Ni	Co	Mn	S	Total
<0.01	0.01	<0.01	0.03	<0.01	0.01	0.01	0.12	0.01	<0.01	0.01	53.38	101.35
<0.01	0.03	<0.01	0.07	<0.01	0.01	0.01	0.07	0.01	<0.01	0.01	53.86	100.17
<0.01	<0.01	<0.01	<0.01	<0.01	<0.01	0.02	0.16	0.01	<0.01	0.01	38.65	100.04
<0.01	0.01	0.01	0.01	<0.01	0.01	0.01	0.06	0.01	<0.01	0.15	32.36	101.36
86.37	0.14	0.02	0.01	0.05	0.10	<0.01	0.30	<0.01	0.01	0.01	13.69	101.15
<0.01	0.02	<0.01	42.96	0.01	0.11	0.04	0.07	0.01	<0.01	0.01	20.99	100.60
<0.01	0.33	<0.01	18.92	1.69	<0.01	0.02	0.15	<0.01	<0.01	0.02	27.51	99.33
<0.01	3.57	0.01	4.30	23.02	<0.01	<0.01	0.07	0.01	<0.01	0.02	24.75	98.89
<0.01	14.70	<0.01	0.09	27.26	<0.01	<0.01	0.07	<0.01	0.01	0.02	23.40	98.84
<0.01	0.03	<0.01	0.01	0.01	0.01	0.01	0.10	<0.01	<0.01	<0.01	34.22	99.48
<0.01	0.05	0.01	0.04	0.01	0.01	0.02	0.09	0.01	0.01	0.01	32.57	99.69
<0.01	0.02	0.02	<0.01	0.01	0.01	<0.01	0.05	<0.01	<0.01	<0.01	22.15	99.13
<0.01	0.15	<0.01	16.66	0.14	0.03	0.01	0.26	0.01	0.01	0.01	31.32	97.54
0.27	1.91	95.81	0.02	0.01	0.01	<0.01	0.02	<0.01	<0.01	<0.01	0.08	98.53
0.42	4.99	91.95	0.05	0.01	0.02	<0.01	0.01	<0.01	<0.01	<0.01	0.33	98.35
0.46	92.81	0.02	0.08	0.02	0.12	0.02	0.06	<0.01	<0.01	<0.01	0.10	94.08
<0.01	0.12	0.03	0.03	<0.01	0.00	0.07	0.02	<0.01	<0.01	<0.01	2.78	100.42
21.77	0.02	<0.01	6.22	<0.01	0.02	<0.01	0.06	<0.01	<0.01	<0.01	3.63	56.33
0.56	0.02	<0.01	0.69	<0.01	0.04	<0.01	<0.01	<0.01	<0.01	<0.01	0.12	61.46

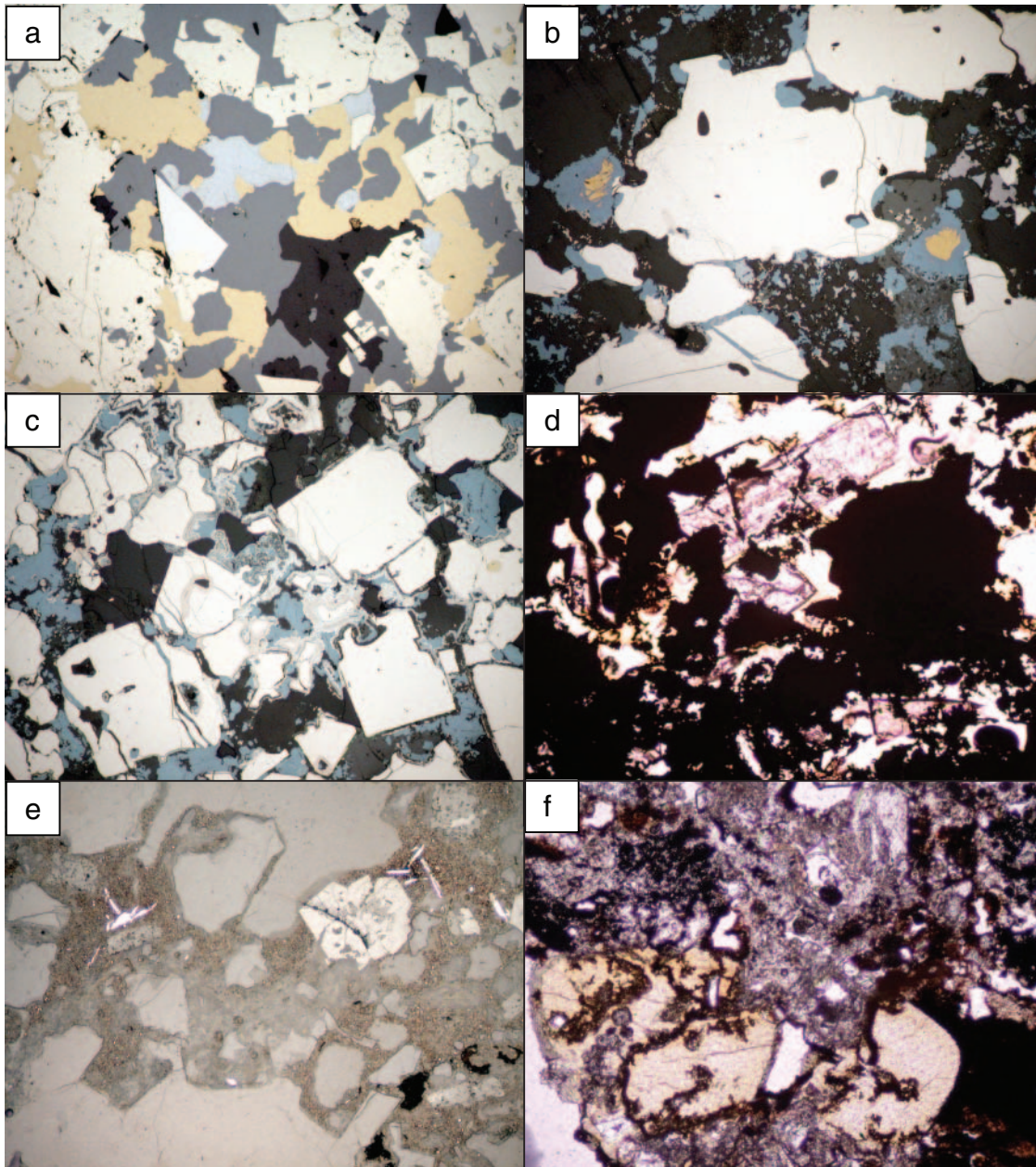


FIG. 9. Photomicrographs of primary and supergene sulfide ore. a. Triangular arsenopyrite (white) overgrowing pyrite (cream) intergrown with sphalerite (dark gray), chalcopyrite (beige), galena (light blue), and gangue (black; B121-267-1, 100 \times magnification, reflected light, field of view = 1.15 mm). b. Remnants of chalcopyrite (yellow) in digenite patches (blue) with anhedral pyrite (white) in gangue (dark gray); note medium-gray anglesite overgrown by digenite in right corner (B-POL-31-3, 80 \times magnification, reflected light, field of view = 1.44 mm). c. Colloidal secondary pyrite rimming pyrite cubes in digenite matrix (B-POL-32-5, 80 \times magnification, reflected light, field of view = 1.44 mm). d. Euhedral anglesite crystals growing into void in digenite matrix (B-POL-31-7, 90 \times magnification, transmitted light, field of view = 1.28 mm). e. Hematite needles with euhedral anglesite in matrix (B67-48-8, 70 \times magnification, reflected light, field of view = 1.64 mm). f. Yellow Pb-Zn-siderite veined by colloidal SiO₂ overgrowing barite-anglesite in vesicular matrix (B67-48-9, 90 \times magnification, transmitted light, field of view = 1.28 mm).

relatively flat REE patterns (e.g., La_N/Yb_N <5) and low Zr/Y values (e.g., Zr/Y <5) for the rhyolites, dacites, and granites indicate a tholeiitic affinity for these felsic rocks, whereas the feldspar porphyry dike suite is calc-alkalic (Leshner et al., 1986; Barrett and MacLean, 1999).

Most of the less-altered basalts have 44 to 54 wt percent SiO₂, 0.8 to 1.8 percent TiO₂, 4 to 8 wt percent MgO, 50 to

100 ppm Zr, and relatively flat REE patterns, with La_N/Yb_N from 1 to 3.5 (Fig. 11c). Gabbroic rocks from the Bisha Gabbroic Complex and from sills intercalated with the footwall strata are compositionally similar to the basalts, and both plot in the tholeiitic fields in conventional ternary diagrams (e.g., AFM diagram of Irvine and Baragar, 1971; Jensen cation plot of Jensen, 1976). On average the gabbro samples have higher

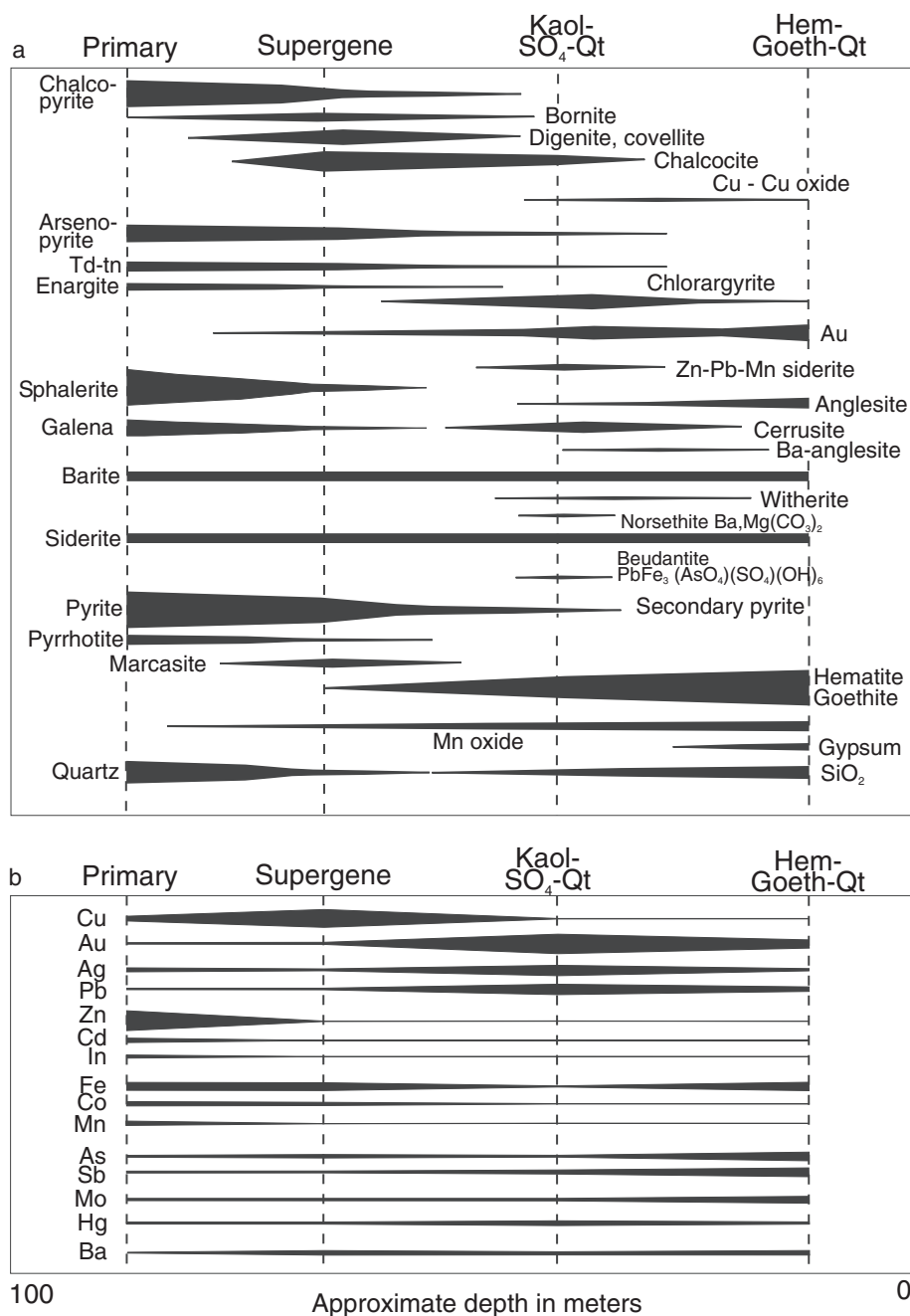


FIG. 10. Schematic mineral paragenetic sequence and metal distribution for main mineralization types. a. Mineralogical paragenetic sequence. Primary barite is present in primary and supergene massive sulfide, whereas it is commonly secondary and with replacement textures in the kaolinite-sulfate-quartz (Kaol-SO₄-Qt) and hematite-goethite-quartz (Hem-Goeth-Qt) zones. b. Metal distribution. Gallium is present at ~50 ppm level in all types.

TiO₂, a reflection of the presence of cumulus oxide phases. The sills may represent feeders to the basalts (Fig. 11c). The similar compositions of the gabbro and basalt are permissive of a cogenetic relationship, where the gabbroic rocks could represent mesocumulates derived by fractionation from the basaltic composition (e.g., Barrie et al., 1991). The average least altered basalt composition is shown in a primitive mantle-normalized plot in comparison to average mid-ocean ridge basalts (MORB) and E-MORB in Figure 12. The plot

indicates that the basalts either came from an enriched mantle source or that they have undergone some crustal contamination en route to the surface, or both. The negative Nb anomaly indicates an arc signature for these rocks (e.g., Hawkesworth et al., 1993).

To summarize, the basalts, rhyolites, and volumetrically minor dacites, as well as gabbroic and granitic rocks within the strata have trace element signatures that indicate tholeiitic to transitional tholeiitic affinities, whereas feldspar

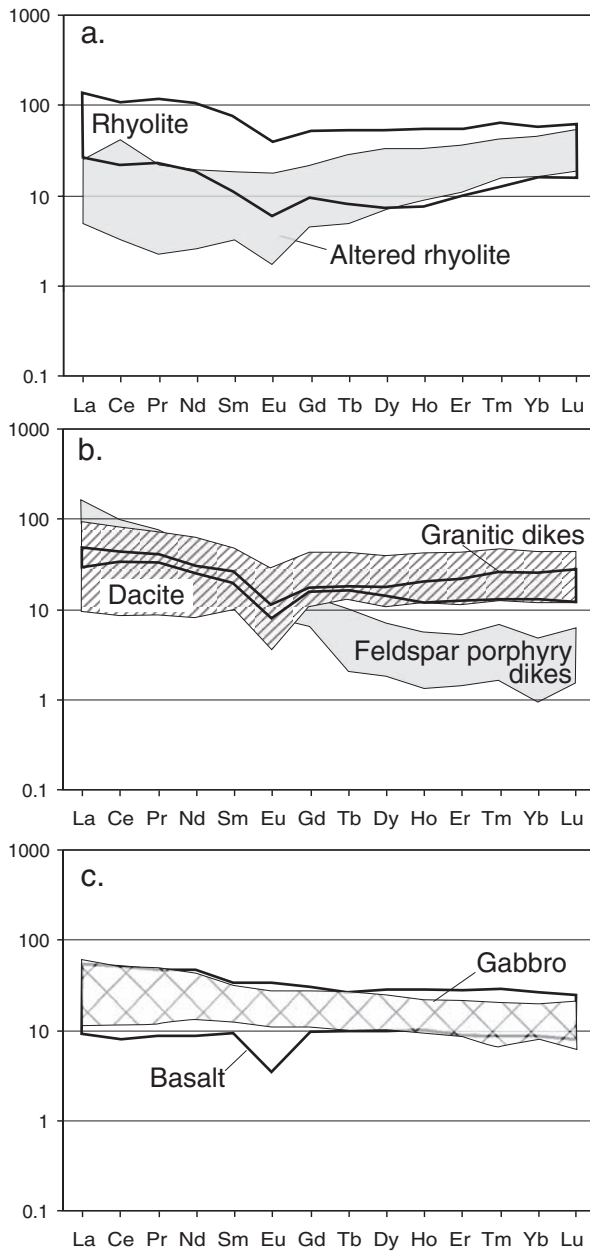


FIG. 11. Chondrite-normalized (using values of Taylor and Gorton, 1977) rare earth element profile ranges for selected surface whole-rock samples from Bisha. a. Dacite, $n = 22$; feldspar porphyry dikes, $n = 6$; and granite, $n = 2$. b. Rhyolite, $n = 138$; altered rhyolite, $n = 14$; c. basalt, $n = 37$; gabbro, $n = 5$.

porphyry dikes are clearly calc-alkalic. "Tholeiitic" FIII rhyolites (Leshner et al., 1986) or high-silica, high-temperature rhyolites (Barrie, 1995) are preferentially associated with VMS deposits in primitive greenstone belts.

Alteration geochemistry: chlorite alteration index and europium mobility

Footwall chlorite alteration is common at Bisha, as it is in many VMS systems (e.g., Kranidiotis and MacLean, 1987; Barrett and MacLean, 1999; Gemmill and Fulton, 2001). Chloritization of volcanic rocks by moderate- and high-temperature hydrothermal fluids is manifested geochemically in

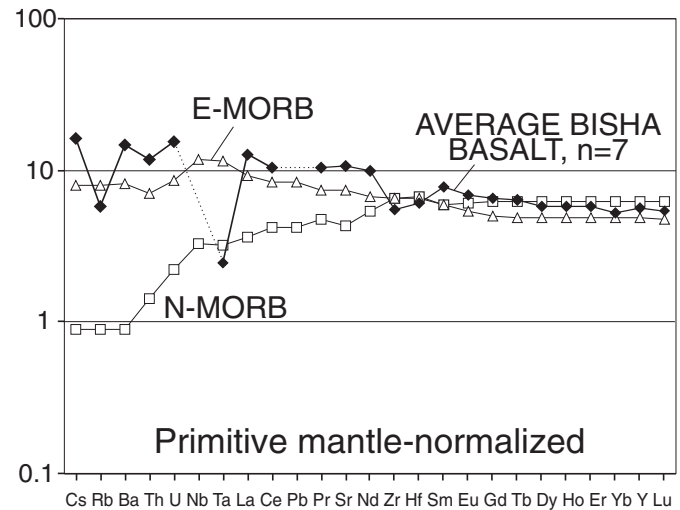


FIG. 12. Primitive mantle-normalized (using values of Sun and MacDonough, 1989) profiles for seven least altered basalt samples from south- and northeast of the Bisha deposit. The average basalt composition at Bisha includes data for Th and U which are accurate to only $\sim \pm 1$ ppm; however the average values are reasonable. The average basalt composition is similar to modern E-MORB but with higher large ion lithophile and light REE contents, which may reflect a crustal component.

several ways, notably by higher volatile contents or loss on ignition (LOI) in alkali and alkaline earth element and/or oxide depletion and by a gain in magnesium and iron. A chlorite alteration index: $(\text{MgO} + \text{Fe}_2\text{O}_3) \cdot 100 / (\text{MgO} + \text{Fe}_2\text{O}_3 + \text{CaO} + \text{Na}_2\text{O} + \text{K}_2\text{O})$ is an effective means to document footwall chlorite alteration. This index is similar to other alteration indices (e.g., Hashimoto index: Ishikawa et al., 1976; chlorite index: Saeki and Date, 1980) but presents the strength of magnesium and iron addition (+chlorite+pyrite) and alkali depletion as a number from 0 to 100. At Bisha, pervasive chlorite alteration in footwall tuffs extends the entire length of the deposit along its eastern side (Fig. 13). In contrast, hanging-wall altered rhyolites to the west of the Bisha and Bisha Northwest deposit horizon are commonly silicified, with 80 to 85 wt percent SiO_2 , and sodium enrichment (up to 4–5 wt % Na_2O) is present away from the Bisha deposit, to the west, north, and south from 500 m to several kilometers. This may represent pervasive and more regional low-temperature albittization related to the late stages of hydrothermal circulation in the volcanic-sedimentary stratigraphy after VMS deposition.

A downhole, whole-rock major and trace element traverse across the eastern lens shows footwall versus hanging-wall elemental and oxide enrichments and depletions, as exemplified by the europium anomaly (Fig. 14, App. 2). Values of greater than one are positive Eu anomalies on chondrite normalized plots. Positive anomalies are uncommon in igneous rocks and are generally limited to plagioclase-rich rocks such as anorthosites and plagioclase phyric basalts, as Eu^{2+} is preferentially incorporated into the plagioclase crystal structure (e.g., Weill and Drake, 1975). Europium is generally immobile, but in low pH hydrothermal fluids at $>250^\circ\text{C}$ it can become mobile as a divalent cation (Michard, 1989). Europium mobility has been noted in subsea-floor hydrothermal systems

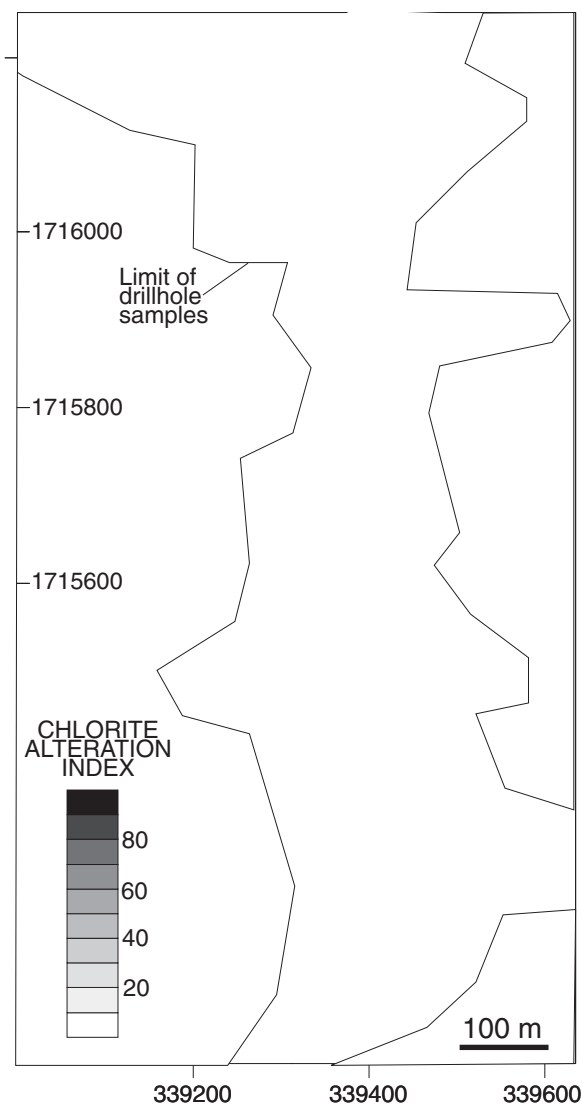


FIG. 13. Contoured chlorite alteration index for whole-rock samples from drill core ($n = 420$) projected to surface, along with the outline of the massive sulfide below the gossan. The index is $(\text{MgO} + \text{Fe}_2\text{O}_3(\text{total}))^*100/(\text{MgO} + \text{Fe}_2\text{O}_3(\text{total}) + \text{CaO} + \text{Na}_2\text{O} + \text{K}_2\text{O})$, in wt percent. This index highlights strong chlorite alteration in the stratigraphic footwall east of the eastern lens for its entire length and west of the western lens at the north end, on the opposite side of the overturned fold.

(e.g., Lottermoser, 1989) and in older VMS systems (Campbell et al., 1984; Barrie and Taylor, 2001), and Eu enrichment can be present in paleosea-floor precipitates or exhalites (Barrie et al., 2005). At Bisha, europium is depleted in the footwall and has been added to the hanging wall (Fig. 14). The footwall depletion and hanging-wall enrichment is mirrored to varying degrees by the distribution of alkali and alkaline earth elements, including sodium, calcium, and potassium, strontium, and barium (App. 2).

Galena and anglesite lead isotope data and model ages

Lead isotope analyses of galena and cerrusite-anglesite mineral separates provide constraints on the age and genesis of the Bisha deposit and other deposits in the region. Two galenas from Bisha primary massive sulfide have crustal

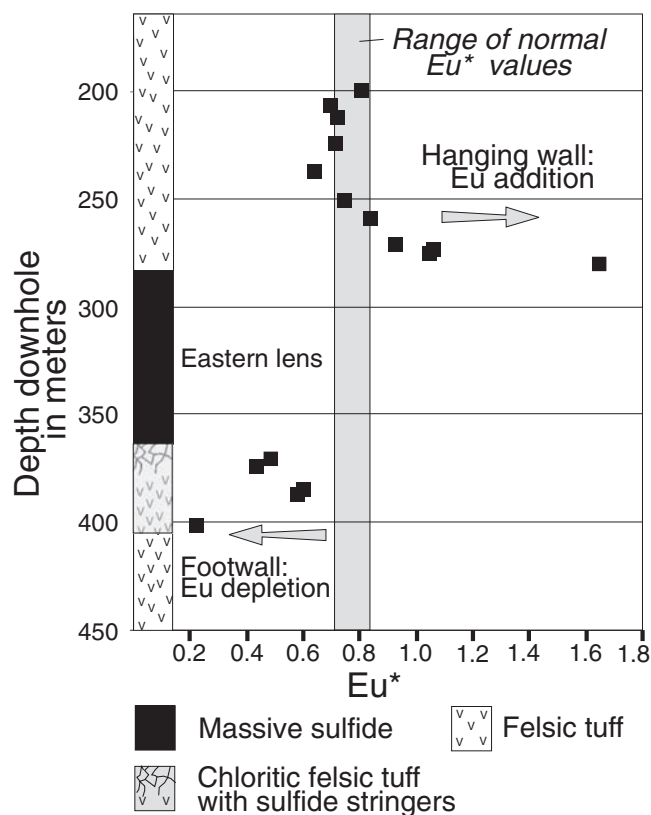


FIG. 14. Europium anomaly $(\text{Eu}^*/\text{Eu}^*)_{\text{norm}} = (\text{Eu}^*/\text{Eu}^*)_{\text{meas}} / [(\text{Sm}/0.0722) + (\text{Gd}/0.259)]$ vs. stratigraphic height for DDH B-164, 50 m south of the cross section in Figure 6. The eastern lens has a true thickness of 65 m here. The chlorite-altered footwall downhole and to the east has significant europium depletion, whereas a strong positive europium anomaly is present in the immediate hanging wall to the west.

model ages of 782 and 790 Ma, and two cerrusite-anglesite mineral separates from the Bisha kaolinite-quartz-sulfate zone have model ages of 784 and 778 Ma, using Stacey and Kramers (1975) terrestrial (crustal) lead model (Table 4, Figs. 15, 16). Galenas from VMS deposits at Bisha Northwest, Harena, and for the Adi Nefas deposit in the eastern Nakfa terrane near Asmara, Eritrea, ~170 km to the east, were also analyzed. These yielded model ages of 776, 773, and 720 Ma, respectively; although it is noted that the Stacey and Kramers model does not fit as well for Adi Nefas. A linear regression of the four galena samples from the Bisha VMS district yields an intersection with the Stacey and Kramers growth curve of 810 Ma but with a very high MSWD of 373 (York least squares regression model 1: scatter assumed to be due to analytical error). If the two cerrusite-anglesite samples are included with the Bisha district galenas, the regression age is 781 Ma, with a very high MSWD (1620, York least squares regression model 1 intersects the growth curve at 781 Ma). The two carbonate and/or cerrusite samples alone form a line with a younger intercept at 717 Ma. The mean of the six samples from the Bisha VMS district is 780.5 Ma ($1\sigma = 6.1$ Myrs), and this is interpreted as the best age estimate for the deposits in the district. The Okreb galena sample, from a late tectonic, granite-related quartz sulfide gold vein, 12.5 km southeast from Bisha, is significantly younger at 493 Ma (Fig. 15).

TABLE 4. Pb Isotope Data for the Bisha Deposit and Other Deposits of the Nakfa Terrane¹

Deposit	Sample no. and description	²⁰⁸ Pb/ ²⁰⁴ Pb		²⁰⁶ Pb/ ²⁰⁴ Pb		²⁰⁷ Pb/ ²⁰⁴ Pb		Stacey and Kramers (1975) model age	μ ³
		corrected	2 sigma	corrected	2 sigma	corrected	2 sigma		
Bisha	B21-267 galena ² in primary massive sulfide	36.966	0.003	17.366	0.001	15.514	0.002	782	9.615
	B225-228 galena in primary massive sulfide	36.985	0.005	17.370	0.002	15.520	0.002	790	9.642
	B024-78.5 cerrusite - anglesite from kaolinite quartz sulfate zone	37.000	0.012	17.390	0.003	15.525	0.004	784	9.658
	B67-48 cerrusite-anglesite from kaolinite quartz sulfate zone	37.026	0.008	17.406	0.002	15.528	0.002	778	9.665
Harena	H006 galena in primary massive sulfide	36.907	0.006	17.350	0.003	15.503	0.003	773	9.567
Bisha NW	NW005-152 galena in primary massive sulfide	36.934	0.002	17.352	0.001	15.505	0.001	776	9.576
Adi Nefas	Adi Nefas galena in primary massive sulfide	36.896	0.005	17.352	0.001	15.476	0.002	720	9.436
Okreb	OK004-67.4 galena in quartz sulfide gold vein	37.383	0.013	17.833	0.005	15.548	0.005	493	9.602
(standard)	NBS 981	36.716	0.007	16.944	0.003	15.499	0.003	1036	9.723

¹ Analyses by Brian Cousens, Carleton University, Ottawa, Canada

² Galena separated by panning crushed sulfide or plucking from drill core

³ Calculated ²³⁸U/²⁰⁴Pb using Stacey and Kramers (1975) model

Lead isotope signatures for these deposits are shown with the Stacey and Kramers (1975) terrestrial growth curve and the Doe and Zartman (1979) upper crustal and mantle growth curves, along with fields for Neoproterozoic VMS in Saudi Arabia (Stacey et al., 1982) and other Pan African, Neoproterozoic-hosted massive sulfide deposits in Namibia and Zambia (Kamona et al., 1999) in Figure 16. The ²⁰⁶Pb/²⁰⁴Pb ratios from Bisha are also similar to the most primitive analyses reported for the Ariab VMS Au district, 250 km to the north, in eastern Sudan (Marcoux et al., 1989; only ²⁰⁶Pb/²⁰⁴Pb ratios reported) and broadly along strike with the western Nakfa terrane. The Adi Nefas analysis has a lower ²⁰⁷Pb/²⁰⁴Pb ratio than the Bisha analyses and plots in the field of the Arabian VMS. Initial galena lead isotope work on other VMS in the

eastern Nakfa terrane (Barrie et al., in prep.) also plot within the Arabian VMS field. To summarize, the Bisha VMS district, representing the western Nakfa terrane, has a slightly more evolved (e.g., higher μ: ²³⁸U/²⁰⁴Pb) lead isotope signature than the Asmara VMS district representing the eastern Nakfa terrane and is also more evolved than the Arabian VMS and their host rocks. The Stacey and Kramers (1975) terrestrial (crustal) lead evolution curve closely approximates the Bisha VMS district; however, a more primitive lead evolution model may be more applicable to the eastern Nakfa terrane and the Arabian shield (e.g., lower ²³⁸U/²⁰⁴Pb or earlier separation from chondritic reservoir or both).

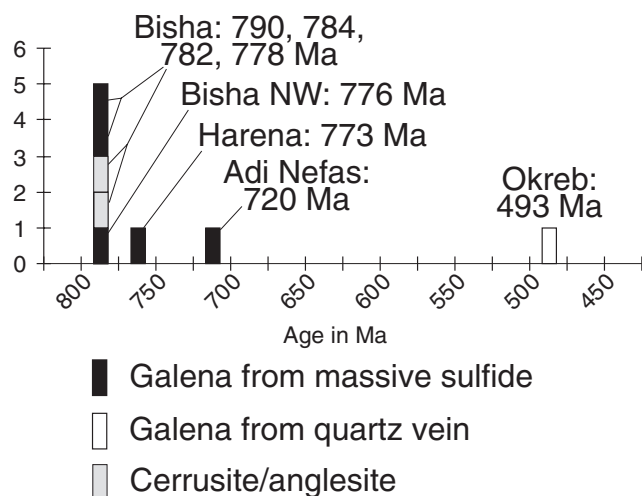


FIG. 15. Histogram of lead isotope model ages for Bisha and other deposits in the region, calculated using Stacey and Kramers (1975) terrestrial lead model.

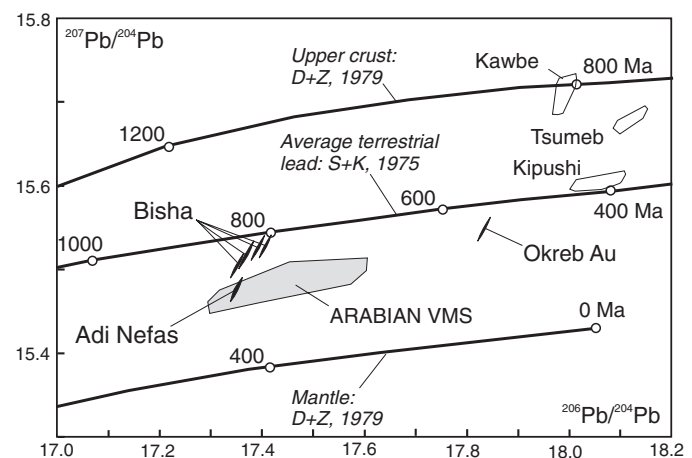


FIG. 16. Lead isotope ratio plot for galena samples from Bisha, Adi Nefas, and Okreb, along with lead growth curves for Stacey and Kramers (1975) average terrestrial lead and Doe and Zartman (1979) upper crust and average mantle. Also plotted are fields for Arabian VMS, including Nuqrah, Jabal Sayid, Wadi Shwas, and Kutam (Stacey et al., 1982) and Neoproterozoic massive sulfide deposits from the Damaran-Lufilian belt (Kawbe and Kipsli, Zambia) and Tsumeb, Namibia (Kamona et al., 1999).

Discussion

Metal contents in primary massive sulfide

Normalized diagrams are a common method to compare elemental abundances between different rocks, ores, or reservoirs and are used here to characterize the Bisha primary massive sulfide metal contents. Barrie and Hannington (1999) used normalized Cu, Pb, Zn, Au, and Ag values to show that there are distinct patterns for five VMS types and that, to a degree, these vary systematically through time. The average metal contents for Bisha primary massive sulfide are shown in comparison to two other bimodal-siliciclastic VMS deposits, a Paleoproterozoic deposit at Ruttan, Manitoba (Barrie et al., 2005), and an average for deposits along the Brunswick horizon in the Ordovician Bathurst camp, New Brunswick (Goodfellow and McC 2003), using an extended primitive mantle-normalized diagram (Fig. 17). The metals are ordered on the basis of their abundance in the average crust. Lead, a very large cation (1.75 Angstroms) that is highly incompatible in the mantle and partitions into crustal melts that form much of the crust, plots to the far left; iron, cobalt, and arsenic are very compatible in mantle silicates and sulfides and plot to the right. The principal ore metals are enriched 2.5 to 3 orders of magnitude in comparison to the average continental crust, and this enrichment is largely attributable to leaching, transport, and deposition of these metals by VMS-forming hydrothermal fluids (Barrie and Hannington, 1999; Seyfried et al., 1999).

For the most part, the average primary massive sulfide from Bisha plots between Ruttan, which is relatively metal poor, and the Brunswick average. The exceptions are for Cd, Au, Zn, and Fe, which are higher than in both of the other bimodal-siliciclastic VMS systems. The Brunswick average has higher Pb (1.86 wt %), Sb (114 ppm), and Sn (338 ppm) contents, and lower Co (343 ppm) and As (2702 ppm; Goodfellow and McCutcheon, 2003), which is consistent with a

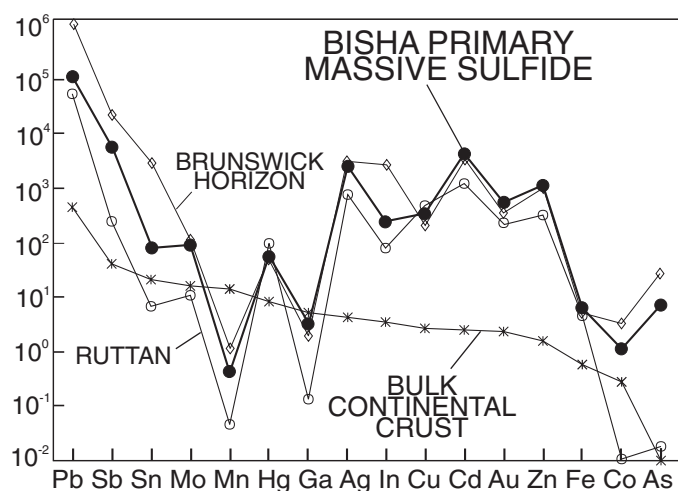


FIG. 17. Average primitive mantle-normalized metal concentrations in Neoproterozoic Bisha primary massive sulfide, in comparison to bulk continental crust and two other bimodal-siliciclastic VMS deposits (average Paleoproterozoic Ruttan massive sulfide: Barrie et al., 2005; average Ordovician Brunswick horizon ores: Goodfellow and McCutcheon, 2003). Primitive mantle and bulk continental crust values are listed in Barrie et al. (2005).

greater crustal influence, probably due to a higher proportion of sedimentary or felsic strata (or both) in the footwall. The higher lead at Brunswick and the lower lead at Ruttan could also reflect, in part, a temporal increase in lead over time due to radiogenic decay from uranium and thorium.

All three deposits have relatively low manganese contents (Fig. 17). Although manganese is highly soluble in low pH, reduced hydrothermal fluids, most manganese forms oxyhydroxides after passing through the VMS depositional environment and into the seawater column. Thus, manganese is commonly found with exhalites along strike with VMS deposits (e.g., Iberian Pyrite Belt: Carvalho et al., 1999). Bedrock samples of minor exhalite units extending along strike to the south and southeast for 4 km from Bisha contain 0.5 to 1.4 wt percent Mn ($n = 7$; Nevsun internal report, 2005). Furthermore, soil samples with significantly anomalous manganese are present both south and north of the deposit along strike, in contrast to soil samples over the deposit which are mostly <0.05 wt percent Mn. These data are consistent with manganese passing through the Bisha hydrothermal system and being deposited in exhalites on the paleosea floor along strike.

The average gallium content of the Bisha samples is also low in comparison to other metals (Fig. 17). Gallium is a small trivalent cation that does not easily form sulfide complexes (Wood and Samson, 2005). It is generally immobile, with enrichments of up to only hundreds of ppm in residual bauxite deposits, and up to ~50 to 200 ppm in some VMS deposits (gallium is recovered as a byproduct from both: Kramer, 2006).

In the absence of fluid inclusion data, the composition of the hydrothermal fluid responsible for transport and deposition of metals in the Bisha VMS deposit can be estimated by considering the equilibrium mineral assemblages in the primary sulfide ore and by comparisons with other, well-documented VMS systems, like Kidd Creek, Ontario. An equilibrium, primary mineral assemblage containing low iron sphalerite, pyrite (dominant), pyrrhotite (minor), siderite and muscovite and/or sericite is consistent with a low f_{O_2} hydrothermal fluid with a pH of 3 to 6, and depositional temperatures of 250° to 275°C (e.g., see Hannington et al, 1999).

Metal contents in supergene sulfide, kaolinite-quartz-sulfate, and oxide zones

As noted above, there are significant enrichments of copper in the supergene sulfide zone, and of lead, gold, and silver in the kaolinite-quartz-sulfate and oxide zones, in comparison to the primary massive sulfide. These enrichments reflect: (1) the fixation of oxidation products as insoluble minerals at or above the oxidation boundary; (2) reprecipitation of metal ions in a slightly reducing environment due to the change of the electronic potential; and (3) replacement of a sulfide by another sulfide under reduced conditions but with slightly higher potential to prevent the formation of native metals (Sato, 1992). Near the oxidized upper part of the water table, Cu^{2+} reacts with sulfur or hydrogen sulfide to form covellite (CuS) or chalcocite (Cu_2S), depending on the abundance of copper and the redox potential. If there is excess copper under more oxidizing conditions, chalcocite predominates, as covellite takes on extra Cu^{2+} . For downward-migrating,

copper-saturated fluids, chalcocite generally forms above covellite under slightly oxidized conditions; this is broadly true at Bisha (Fig. 10). Pyrite plays a dual role in that it acts as host for copper deposition as its ferric ions are replaced by copper ions, and its relatively high solubility in the oxidizing environment frees sulfur into the ground water, which lowers the ground-water pH and leads to the dissolution of chalcopyrite and other base metal sulfides (Guilbert and Park, 1986).

One-dimensional, physiochemical fluid-flow models have been developed that simulate supergene copper enrichment in an oxidizing, near-surface environment (Ague and Brimhall, 1989; Shang et al., 2001). Using reasonable assumptions for porosity and Darcy fluid flow from the surface downward (e.g., rain water percolation), Ague and Brimhall (1989) found that bornite formed at the expense of chalcocite and covellite in the supergene blanket zone just below the ground-water table after ~6,000 years, coincident with the formation of kaolinite after feldspars. Redox controlled reactions were used almost exclusively and simulated the copper profile very closely, indicating that other processes for copper deposition, including kinetic reactions and microbial reactions (e.g., Sillitoe et al., 1996) are probably second-order effects. At Bisha, supergene processes may have been operative over very long time periods, as arid conditions have existed for millions of years in this area, evidenced by thick laterites and saprolitic soils below mid-Oligocene flood basalts in the region (Mohr, 1971).

Zinc sulfide is significantly more soluble than lead and copper sulfides in the oxidized, low pH ground-water environment (Guilbert and Park, 1986) and is more likely to be removed from the deposit area by ground-water transport, unless sequestered by carbonate to form smithsonite. Although there are unusual Zn-Pb-Fe carbonate and sulfate minerals present in the kaolinite-quartz-sulfate and oxide zones (Figs. 9, 10), the overall carbonate and Zn contents are low and evidence for significant fixation of soluble Zn (and Cu) by carbonate is lacking. Zinc is anomalous but low in soil sampling over the deposit as well (W.F. Nielson and C. Ausant, unpub. report for Nevsun Resources, 2005, 350 p.). It would appear that Zn has largely been removed from the oxidized upper zones of the deposit over time. In contrast, lead and barium form the relatively stable sulfates, anglesite, and barite, respectively, and are enriched in the kaolinite-quartz-sulfate and oxide zones.

Gold enrichment in the hematite-goethite gossan is common in weathered and oxidized ore deposits. Gold enrichment in this environment is believed to form by downward weathering, where the gold is derived from decomposition of auriferous sulfides (pyrite in particular), by a combination of chemical, residual, and mechanical processes (Anand, 2001). Gold and silver can be transported as either chloride or aqueous sulfur complexes at low temperatures under oxidizing, low pH conditions and precipitated as native metals with iron oxides. Low pH conditions are indicated by a jarosite and goethite assemblage, which is stable only at pH 1 to 2.5 under oxidizing conditions provided potassium and sulfur are present (Alpers and Brimhall, 1989).

Geotectonic setting

The primary geochemistry of mafic and felsic volcanic rocks and nearby intrusive rocks indicate a largely bimodal

igneous suite, with evidence for cogenetic volcanic and intrusive rocks. The suite has tholeiitic to transitional calc-alkalic affinities, with mantle plume-influenced, primitive arc signatures for least altered basalts. The lead isotope signatures for galenas and anglesite from the Bisha, Bisha Northwest, and Harena deposits have model ages that range from 790 to 770 Ma and plot very close to the Stacey and Kramers (1975) terrestrial (crustal) growth curve. These data indicate that the deposits and their host rocks formed early during the development of the 800 to 550 Ma Nakfa terrane, and, along with other radiogenic isotope studies (Teklay, 1997; Teklay et al., 2002; Andersson et al., 2006), they are consistent with minimal or no contribution from an older crustal component. The lead isotope data from the Bisha district, with their higher μ ($^{238}\text{U}/^{204}\text{Pb}$) values, are distinct from those of both the eastern Nakfa terrane and the Arabian shield VMS, indicating a distinct provinciality for Bisha and perhaps for the western Nakfa terrane. Further galena lead isotope studies constrained by U-Pb zircon ages for host volcanic rocks can test whether the Nakfa terrane should be considered as two (or more) separate terranes.

Summary and Conclusions

The Bisha VMS deposit and nearby VMS deposits, Bisha Northwest, Harena, and Hambok, form a newly discovered VMS district in the Neoproterozoic Nakfa terrane of western Eritrea. The Bisha deposit is a large (total resources >39 Mt) and relatively rich Zn-Cu-Au-Ag deposit with potentially recoverable Pb, Cd, and Ga.

The deposit is within felsic and intermediate volcanic tuffs and fine-grained siliciclastic rocks; minor quartzites, carbonates, and the very large Bisha Gabbroic Complex are present well downsection. Over half of the stratigraphic column is sedimentary within 3 km of the ore horizon, and the deposit and district are considered bimodal-siliciclastic (cf. Barrie and Hannington, 1999). The immediate stratigraphy forms an overturned synform within a probable, west-over-east, kilometer-scale nappe structure. It would appear that the strata have been folded and thrust against the gabbroic complex which behaved as a competent buttress during deformation.

The volcanic rocks are bimodal and have transitional tholeiite geochemical affinities. Nearby mafic and felsic intrusive rocks, including the gabbroic complex, have similar affinities, and their geochemistry is permissive of a cogenetic, intrusive-extrusive suite. The Bisha Gabbroic Complex may represent a large, high-level heat source for the hydrothermal systems that formed the Bisha and other VMS deposits in the region; this hypothesis remains to be tested rigorously with U-Pb geochronology.

There are four ore types based on mineralogy that occur in distinct zones. Collectively, these reflect supergene, leaching, and oxidation processes in the near-surface environment under arid conditions after primary massive sulfide deposition. From the surface downward, they are as follows: (1) a hematite-goethite-quartz gossan zone, with high gold, silver, and lead contents; (2) a kaolinite-quartz-sulfate zone, also with high gold, silver, and lead contents; (3) a chalcocite-bearing supergene sulfide zone, with high copper contents; and (4) primary massive sulfide, with high zinc and copper contents.

The average ore and trace metal contents of the primary massive sulfide are similar to those of other bimodal-siliciclastic VMS deposits at Ruttan, Manitoba, and in the Bathurst district, New Brunswick. The ore metal contents are 2.5 to 3 orders of magnitude greater than average continental crust, and variations in the trace metal contents between these deposits are principally due to variations in the composition of footwall host-rock strata. The low manganese content of the primary ore is complimentary to high manganese contents in soil samples broadly along strike, reflecting primary manganese dispersion on to the paleosea floor for one to two km along strike from the Bisha hydrothermal system.

An average Stacey and Kramers (1975) terrestrial model age for the Bisha VMS district, based on lead isotope analyses of six galena and anglesite mineral separates representing the Bisha, Bisha Northwest, and Harena deposits, is 780.5 Ma ($1\sigma = 6.1$ m.y.). This is ~60 m.y. older than a lead isotope crustal model age for Adi Nefas in the Asmara VMS district of the eastern Nakfa terrane. Thus, the Bisha VMS district formed in a plume-influenced, transitional tholeiitic arc environment during the early stages of development of the Nakfa terrane in western Eritrea.

Acknowledgments

This work follows the discovery of the Bisha deposit by a team of geologists, including the second author, and a small private resource company (Ophir Ventures) that drew attention to the area in 1996. The team of B. Nielsen and J. Clarke should be credited with this discovery, from prospecting through initial drilling. We thank J. Clarke, President of Nevsun Resources, Alem Kibreab, Deputy Minister of Mines, and the Eritrean Ministry of Mines and Petroleum Resources for their support. Brian Cousens and Ingrid Kjarsgaard are thanked for analytical work with lead isotope analyses and microprobe analyses, respectively. We also thank Craig Scherba of Taiga Consultants, who provided invaluable assistance with drafting and data management, and Daouda Ouattara, David Daoud, and Charlie Greig for geologic contributions and ideas. Garry Davidson and an anonymous reviewer provided insightful comments on an earlier version of this manuscript on behalf of *Economic Geology* and these efforts are appreciated.

August 9, 2006; July 12, 2007

REFERENCES

- Ague, J.J., and Brimhall, G.H., 1989, Geochemical modeling of steady state fluid flow and chemical reaction during supergene enrichment of porphyry fluid flow and chemical reaction during supergene enrichment of porphyry: *ECONOMIC GEOLOGY*, v. 84, p. 506–528.
- Alpers, C.N., and Brimhall, G.H., 1989, Paleohydrologic evolution and geochemical dynamics of cumulative supergene metal enrichment at La Escondida, Atacama desert, northern Chile: *ECONOMIC GEOLOGY*, v. 84, p. 229–256.
- Anand, R.R., 2001, Evolution, classification and use of ferruginous regolith materials I. Gold exploration, Yilgarn craton, Western Australia: *Geochemistry: Exploration, Environment, Analysis*, v. 1, p. 221–236.
- Andersson, U.B., Ghereab, W., and Teklay, M., 2006, Crustal evolution and metamorphism in the east-central Eritrea, south-east Arabian-Nubian shield: *Journal of African Earth Sciences*, v. 44, p. 45–65.
- Barrett, T.J., and MacLean, W., 1999, Volcanic sequences, litho-geochemistry, and hydrothermal alteration in some bimodal volcanic-associated massive sulfide deposits: *Reviews in Economic Geology*, v. 8, p. 101–132.
- Barrie, C.T., 1995, Zircon thermometry of high temperature rhyolites near volcanic-associated massive sulfide deposits, Abitibi subprovince, Canada: *Geology*, v. 23, p. 169–172.
- Barrie, C.T., and Hannington, M.D., 1999, Volcanic-associated massive sulfide deposits: Processes and examples in modern and ancient settings: *Introduction: Reviews in Economic Geology*, v. 8, p. 1–11.
- Barrie, C.T., and Taylor, C., 2001, Geology of the Ruttan VMS deposit in the southern Rusty Lake volcanic belt, northern Manitoba: *Manitoba Mines Branch Open File Report*, 29 p.
- Barrie, C.T., Hart, T.R., Gorton, M.P., and Naldrett, A.J., 1991, Geochemistry and petrogenesis of the Kamiskotia gabbroic complex and related bimodal volcanic rocks, Abitibi subprovince, Ontario: *Precambrian Research*, v. 50, p. 173–199.
- Barrie, C.T., Taylor, C.F., and Ames, D.E., 2005, Geology and metal contents of the Ruttan volcanogenic massive sulfide deposit, northern Manitoba, Canada: *Mineralium Deposita*, v. 39, p. 795–812.
- Berhe, S., 1990, Ophiolites in northeast and east Africa: Implications for Proterozoic crustal growth: *Journal of the Geological Society of London*, v. 147, p. 41–57.
- Campbell, I.H., Leshner, C.M., Coad, P., Franklin, J.M., Gorton, M.P., and Thurston, P.C., 1984, Rare earth element mobility in alteration pipes below massive sulfide deposits: *Chemical Geology*, v. 45, p. 181–202.
- Carvalho, D., Barriga, F.J.A.S., and Munhá, J., 1999, Bimodal-siliciclastic systems—the case of the Iberian Pyrite Belt: *Reviews in Economic Geology*, v. 8, p. 375–408.
- Doe, B.R., and Zartman, R.E., 1979, Plumbotectonics, I. The Phanerozoic, in Barnes, H.L., ed., *Geochemistry of hydrothermal ore deposits*, 2nd ed.: New York, John Wiley and Sons, p. 22–70.
- Drury, S.A., and de Sousa Filho, C.R., 1998, Neoproterozoic terrane assemblages in Eritrea: Review and prospects: *Journal of African Earth Sciences*, v. 27, p. 331–348.
- Franklin, J.M., Gibson, H.L., Jonasson, I.R., and Galley, A.G., 2005, Volcanogenic massive sulfide deposits: *ECONOMIC GEOLOGY 100TH ANNIVERSARY VOLUME*, p. 523–560.
- Gemmell, J.B., and Fulton, R., 2001, Geology, genesis, and exploration implications of the footwall and hanging-wall alteration associated with the Hellyer volcanic-hosted massive sulfide deposit, Tasmania, Australia: *ECONOMIC GEOLOGY*, v. 96, p. 103–1035.
- Goodfellow, W.D., and McCutcheon, S.R., 2003, Geologic and genetic attributes of volcanic sediment-hosted massive sulfide deposits of the Bathurst mining camp, northern New Brunswick—a synthesis: *ECONOMIC GEOLOGY MONOGRAPH 11*, p. 245–301.
- Guilbert, J.M., and Park, W., 1986, *The geology of ore deposits*: New York, W. H. Freeman, 985 p.
- Hannington, M.D., Kjarsgaard, I., and Bleeker, W., 1999, Sulfide mineralogy, geochemistry and ore genesis of the Kidd Creek deposit. Part I. The North, Central, and South orebodies: *ECONOMIC GEOLOGY MONOGRAPH 10*, p. 163–224.
- Hawkesworth, C.J., Gallagher, K., Hergt, J.M., and McDermott, F., 1993, Mantle and slab contributions in arc magmas: *Annual Reviews of Earth and Planetary Sciences*, v. 21, p. 175–204.
- Irvine, T.N., and Baragar, W.R.A., 1971, A guide to the chemical classification of common volcanic rocks: *Canadian Journal of Earth Sciences*, v. 8, p. 523–548.
- Ishikawa, Y., Sawaguchi, T., Iwaya, S., and Horiuchi, M., 1976, Delineation of prospecting targets for Kuroko deposits based on models of volcanism of underlying dacite and alteration halos: *Mining Geology*, v. 26, p. 105–117.
- Jensen, L., 1976, A new cation plot for classifying subalkalic volcanic rocks: Ontario Department of Mines Miscellaneous Paper 66, 30 p.
- Johan, Z., 1988, Indium and germanium in the structure of sphalerite: An example of coupled substitution with copper: *Mineralogy and Petrology*, v. 39, p. 211–229.
- Kamona, A.F., Leveque, J., and Haack, U., 1999, Lead isotopes of the carbonate-hosted Kabwe, Tsumeb, and Kipushi Pb-Zn-Cu sulphide deposits in relation to Pan African orogenesis in the Damaran-Lufilian fold belt of Central Africa: *Mineralium Deposita*, v. 34, p. 273–283.
- Kramer, D.A., 2006: Gallium: U.S. Geological Survey Commodities Report on Gallium, 2 p.
- Kranidiotis, P., and MacLean, W.H., 1987, Systematics of chlorite alteration at the Phelps Dodge massive sulfide deposit, Matagami, Quebec: *ECONOMIC GEOLOGY*, v. 82, p. 1898–1911.
- Leshner, C.M., Goodwin, A.M., Campbell, I.H., and Gorton, M.P., 1986, Trace element geochemistry of ore-associated and barren felsic metavolcanic

- rocks in Superior province, Canada: *Canadian Journal of Earth Sciences*, v. 23, p. 222–237.
- Lottermoser, B.G., 1989, Rare earth element study of exhalites within the Willyama Supergroup, Broken Hill block, Australia: *Mineralium Deposita*, v. 24, p. 92–99.
- Marcoux, E., Cottard, F., Recouche, G., El Samani, Y., Calvez, J.Y., and Deschamps, Y., 1989, Lead isotope signatures of the polymetallic mineralization in the Ariab District, Red Sea Hills, northeastern Sudan: *Journal of Geochemical Exploration*, v. 32, p. 315–317.
- Michard, A. 1989, Rare earth element systematics in hydrothermal fluids: *Geochimica et Cosmochimica Acta*, v. 53, p. 745–750.
- Mohr, P.A., 1971, *The Geology of Ethiopia: Haile Selassie I*: Addis Ababa, University Press, 268 p.
- Nieto, J.M., Capitán, M.A., Sáez, R., and Almodóvar, G.R., 2003, Beudantite: A natural sink for As and Pb in sulphide oxidation processes: *Transactions of the Institution of Mining and Metallurgy*, v. 112, p. 293–296.
- Reddy, D., and Brisebois, K., 2004, Technical report on the Bisha property and resource estimate of the Bisha deposit, Gash-Barka district, Eritrea: AMEC Canada Ltd. report for Nevsun Resources, 203 p.
- Saeki, Y. and Date, J., 1980, Computer application to the alteration data of the footwall dacite lava at the Ezuri Kuroko deposits, Akita prefecture, *Mining Geology*, v. 30, p. 241–250 (in Japanese with English abstract).
- Sato, M., 1974, Distribution and setting of the Kuroko deposits: *Society of Mining Geologists Japan, Special Issue 6*, p. 1–10.
- Sato, M., 1992, Persistence-field Eh-pH diagrams for sulfides and their application to supergene oxidation and enrichment of sulfide ore bodies: *Geochimica et Cosmochimica Acta*, v. 56, p. 3133–3156.
- Seyfried, W.E., Jr., Ding, K., Berndt, M.E., and Chen, X., 1999, Experimental and theoretical controls on the composition of mid-ocean ridge hydrothermal fluids: *Reviews in Economic Geology*, v. 8, p. 133–156.
- Shang, C., Lin, W.-S., and Liu, C.-W., 2001, A simulation of the supergene copper enrichment process: Republic of China, *Proceedings of the National Science Council*, v. 25, p. 293–299.
- Sillitoe, R.H., Folk, R.L., and Saric, N., 1996, Bacteria as mediators of copper sulfide enrichment during weathering: *Science*, v. 272, p. 1153–1155.
- Stacey, J.S., and Kramers, J.D., 1975, Approximation of terrestrial lead isotope evolution by a two-stage model: *Earth and Planetary Science Letters*, v. 26, p. 207–221.
- Stacey, J.S., Doe, B.R., Roberts, R.J., and Delevaux, M.H., 1982, A lead isotope study of mineralization in the Saudi Arabian Shield: *Contributions to Mineralogy and Petrology*, v. 74, p. 175–188.
- Stern, R., 1994, Neoproterozoic (900–550 Ma) arc assembly and continental collision in the Proterozoic East African orogen: Implications for the consolidation of Gondwanaland: *Annual Reviews of Earth and Planetary Sciences*, v. 22, p. 319–351.
- Sun, S.-S., and MacDonough, W.F., 1989, Chemical and isotopic systematics of oceanic basalts: Implications for mantle composition and processes: *Geological Society of London Special Publication 42*, p. 313–345.
- Taylor S.R., and Gorton, M.P., 1977, Geochemical application of spark source mass spectrography: III. Element sensitivity, precision and accuracy: *Geochimica et Cosmochimica Acta*, v. 41, p. 1375–1380.
- Teklay, M., 1997, Petrology, geochemistry and geochronology of Neoproterozoic magmatic arc rocks from Eritrea: Implications for crustal evolution in the southern Nubian Shield: *Eritrea Department of Mines Memoir 1*, 125 p.
- Teklay, M., Kröner, A., and Mezger, K., 2002, Enrichment from plume interaction in the generation of Neoproterozoic arc rocks in northern Eritrea: Implications for crustal accretion in the southern Arabian-Nubian Shield: *Chemical Geology*, v. 184, p. 167–184.
- Weill, D.F., and Drake, M.J., 1973, Europium anomaly in plagioclase feldspar: Experimental results and semi-quantitative model: *Science*, v. 180, p. 1059–1060.
- Wood, S.A., and Samson, I.M., 2005, The aqueous geochemistry of gallium, germanium, indium and scandium: *Ore Geology Reviews*, v. 28, p. 57–102.

APPENDIX 1

Geochemistry of Bisha Area Rock Types—
Average of Least Altered Samples¹

	Rhyolite	Feldspar porphyry dike	Dacite tuff	Granitic dike	Basalt	BGC gabbro
<i>n</i>	83	7	22	2	7	5
Wt %						
SiO ₂	72.90	70.91	68.78	76.00	49.35	44.12
TiO ₂	0.32	0.29	0.45	0.17	1.07	1.87
Al ₂ O ₃	12.59	13.94	12.41	12.60	15.42	14.92
Fe ₂ O ₃	3.88	2.28	6.32	1.58	11.86	15.31
MgO	1.11	0.39	3.85	0.33	4.44	7.62
MnO	0.09	0.02	0.13	0.04	0.18	0.26
CaO	0.57	0.47	0.45	0.38	7.98	9.44
Na ₂ O	2.15	3.72	0.67	4.94	3.64	2.40
K ₂ O	2.66	3.25	2.21	1.43	0.25	0.70
P ₂ O ₅	0.06	0.07	0.09	0.04	0.22	0.22
Cr ₂ O ₃	0.01	0.01	0.01	0.01	0.01	0.02
LOI	2.23	1.89	3.89	0.47	1.94	2.71
Total	98.58	97.23	99.26	97.97	94.42	99.57
Ppm						
Cs	0.43	1.19	0.32	0.90	0.13	0.50
Rb	36	91	32	51	4	12
Sr	114	333	62	105	228	181
Ba	1285	2721	1361	546	102	280
Th	3.0	15.9	2.9	15.5	1.0	1.1
U	1.3	3.5	1.3	3.8	0.3	0.5
Pb	80	35	36	27	<2	8
Nb	5.5	3.9	4.8	14.0	2.3	4.4
Ta	0.5	0.9	0.5	2.3	<0.5	0.5
Zr	179	192	160	130	61	109
Hf	5.5	5.4	4.9	5.5	nd	3.6
Y	44.7	6.4	38.3	34.6	25.8	34.0
La	17.41	40.57	12.02	12.60	8.79	11.22
Ce	37.51	68.69	26.80	32.85	18.66	26.72
Pr	5.08	7.34	3.57	4.25	2.84	3.96
Nd	22.11	23.39	15.85	17.00	13.43	18.92
Sm	5.46	3.30	4.11	4.45	3.47	4.94
Eu	1.25	0.76	0.84	0.70	1.16	1.42
Gd	5.93	2.73	4.74	4.45	3.89	5.60
Tb	1.10	0.29	0.91	0.85	0.69	1.00
Dy	7.22	1.21	5.88	5.25	4.29	6.20
Ho	1.63	0.20	1.36	1.20	0.96	1.22
Er	5.03	0.59	4.17	3.60	2.79	3.72
Tm	0.79	0.11	0.65	0.60	0.40	0.48
Yb	5.24	0.53	4.30	3.95	2.59	3.38
Lu	0.84	0.10	0.70	0.65	0.40	0.48
Zr/Y	4.0	30.1	4.2	3.8	2.4	3.2
La _N /Yb _N	2.24	51.81	1.89	2.15	2.29	2.24

¹ Analyses by XRF and ICP-MS on fused samples, ALS-Chemex Laboratories, Vancouver, B.C.

APPENDIX 2

Whole-Rock Geochemistry for Altered Felsic-Intermediate Tuff Host Rocks in DDH B-164¹

Average depth in meters	Hanging wall to west										Footwall to east				
	205.39	211.33	223.40	236.65	250.13	258.13	270.03	272.40	274.55	279.35	370.10	373.25	384.13	386.45	400.43
Wt %															
SiO ₂	71.84	66.35	71.01	62.08	64.43	66.36	59.78	67.5	61.5	63.5	56.25	65	69.72	71	63.71
Al ₂ O ₃	12.95	15.57	13.45	17.52	13.24	12.92	13.29	9.75	12.63	11.5	10.88	8.76	10.14	10.33	8.93
Fe ₂ O ₃	3.99	4.84	4.29	4.76	5.77	4.81	5.91	6.1	6.26	6.87	14.84	11.61	7.75	6.68	11.55
CaO	0.88	0.86	1.23	0.36	1.26	1.04	6.27	6.1	7.63	3.15	0.14	0.07	0.04	0.03	0.53
MgO	0.79	0.89	1.27	3.48	4.75	5.48	2.47	1.95	2.9	2.03	9.33	7.11	6.44	5.86	8.27
Na ₂ O	4.6	7.29	1.14	0.44	1.72	0.39	0.42	0.51	0.59	0.18	0.09	0.06	0.15	0.07	0.02
K ₂ O	1.79	0.99	3.6	6.11	2.41	2.59	1.63	0.33	0.48	2.46	0.22	0.25	0.8	1.09	0.04
Cr ₂ O ₃	0.01	0.01	<0.01	<0.01	<0.01	<0.01	<0.01	<0.01	0.02	0.01	0.03	0.13	0.01	<0.01	<0.01
TiO ₂	0.29	0.36	0.3	0.41	0.36	0.36	0.3	0.27	0.29	0.32	0.26	0.19	0.26	0.24	0.22
MnO	0.09	0.16	0.1	0.14	0.1	0.19	3.87	3.01	1.3	0.75	0.19	0.16	0.15	0.13	0.19
P ₂ O ₅	0.05	0.06	0.04	0.06	0.05	0.07	0.07	0.05	0.09	0.03	0.05	0.03	0.02	0.04	0.04
BaO	0.16	0.06	0.24	0.35	0.19	0.38	0.55	0.48	0.76	1.62	0.18	0.16	0.28	0.37	0.01
LOI ²	1.6	1.04	2.05	3.3	4.29	4.17	3.91	2.77	3.96	6.24	6.98	5.4	3.72	3.52	5.32
S ²	0.33	0.54	0.26	0.56	1.23	0.27	3.43	3.46	4.16	4.38	3.77	2.38	0.12	0.12	2.08
Total	99.37	99.02	98.98	99.57	99.8	99.03	101.9	102.3	102.56	103.06	103.31	101.19	99.59	99.48	100.92
Ppm															
La	18.4	23.9	16.4	33.1	16.4	17.9	19.6	15.8	17.4	20.4	3.5	4.3	3.7	5.1	3.3
Ce	42.6	59.2	43	68.9	39.8	42.7	46.1	35.5	38.5	45.2	7.9	9.7	8.3	12	7.4
Pr	5.7	8.1	6	8.8	5.6	5.8	6.2	4.9	5.2	6.1	1.1	1.4	1.2	1.7	1
Nd	25.1	35.5	27.6	37.8	25.7	26.2	28.2	21.4	22.6	26.9	5.4	6.2	5.3	7.5	4.7
Sm	6.7	8.9	7.7	9.2	7.1	7.1	7.5	5.5	5.9	7.5	1.6	1.8	1.6	2.2	1.4
Eu	1.5	2	1.8	1.6	1.6	1.8	2	1.9	2.1	3.7	0.3	0.3	0.3	0.3	0.2
Gd	7.3	9.3	8.3	9.5	7.7	7.5	8.1	5.8	6.4	8.4	2.1	2.3	2.2	2.7	1.7
Tb	1.3	1.6	1.5	1.6	1.4	1.4	1.4	1.1	1.2	1.5	0.4	0.5	0.5	0.6	0.4
Dy	8.5	10	9.1	9.8	9	8.4	8.9	6.6	7.2	8.8	3.1	3.6	4.3	4.5	2.9
Ho	1.9	2.2	2	2.1	1.9	1.8	1.9	1.5	1.6	1.9	0.8	0.9	1.2	1.2	0.8
Er	5.9	6.8	6	6.6	5.9	5.5	5.9	4.2	4.6	4.9	2.7	3.2	3.6	3.7	2.7
Tm	0.9	1.1	0.9	1.1	1	0.9	0.9	0.7	0.7	0.7	0.5	0.5	0.6	0.7	0.5
Yb	5.8	7	6	7.1	5.8	5.6	5.8	4.2	4.7	4.6	3.4	3.6	4.1	4.3	3.3
Lu	0.9	1.1	0.9	1.2	0.9	0.9	0.9	0.7	0.8	0.8	0.6	0.6	0.7	0.8	0.6
Th	3	4	3	4	3	3	3	3	3	2	2	2	3	3	2
U	1.6	1.8	1.4	1.8	1.3	1.2	1.5	1.6	1.9	1.5	1	0.9	1.1	1.1	1
Zr	206	253	207	264	201	181	187.5	164.5	188	146	147.5	133.5	172	171.5	146
Y	50.9	60	53.1	57.1	54.1	50	52.8	37.3	40.5	55.7	22.3	25.7	30.2	30.8	20.9
Hf	6	8	6	8	6	5	6	5	6	4	5	4	5	5	5
Nb	6	7	6	8	6	5	5	5	6	4	4	3	5	5	4
Ta	<0.5	0.5	<0.5	0.5	<0.5	<0.5	<0.5	<0.5	<0.5	<0.5	<0.5	<0.5	<0.5	<0.5	<0.5
Ba	1745	654	2390	3350	1840	3640	6000	5090	8080	>10000	1680	1490	2660	3550	79.1
Cs	0.5	0.6	1.1	2.9	1.1	0.7	0.5	0.1	0.2	0.5	0.1	<0.1	0.1	0.1	<0.1
Rb	28.5	19.2	78.9	129.5	54.3	54	37.6	6.2	10.7	48.3	3.6	3.7	11.8	16.2	0.6
Sr	123	188.5	82.2	29.7	112	43.6	113	135	244	94.7	4.2	3.1	7.1	10.5	4.2
Cu	11	18	14	13	15	11	<5	9	5	23	1805	2150	19	12	2100
Zn	268	296	230	160	112	123	248	138	300	1150	1605	1990	472	594	863
Pb	6	9	7	6	6	10	55	30	33	1725	8	14	<5	<5	6
Ni	10	8	<5	7	<5	5	<5	7	<5	10	5	<5	<5	<5	<5
Co	6.1	5.2	2.5	2.8	4	5.5	2.3	3.1	2.3	3.8	29	24.4	5.1	4.1	22.4
Cr	60	50	50	30	30	20	40	90	70	160	30	50	50	40	50
Ga	19	20	22	27	17	18	16	15	17	30	17	13	14	14	13
Mo	<2	<2	<2	6	<2	<2	<2	<2	<2	6	6	4	2	2	2
Sn	2	2	3	3	2	2	2	2	2	10	1	1	1	1	1
Tl	0.9	0.8	2.3	5.6	2.5	4.1	6.9	2.2	3.2	14.6	1.6	1.3	2.6	3.2	<0.5
W	2	2	6	7	4	3	3	2	<1	2	4	3	4	9	<1
In	0.09	0.12	0.13	0.16	0.09	0.10	0.08	0.06	0.06	0.53	0.19	0.25	0.02	0.03	0.07
Sb	0.9	0.5	0.3	1.3	0.4	0.2	0.5	1.1	1.2	2.6	0.4	0.3	0.1	0.1	0.2
Se	1	1	1	1	<1	<1	<1	1	2	16	8	6	1	1	11
Te	0.05	<0.05	0.07	0.05	<0.05	<0.05	0.36	0.28	0.58	68.8	6.65	4.39	0.06	0.07	2.98

¹ Major element oxides analyzed by XRF, minor and trace elements analyzed by ICP-MS and ICP-AES after lithium metaborate and 4 acid attack; ALS-Chemex Laboratories, Vancouver B.C.

² Loss on ignition may include sulfate